17

Molecular Interactions in Lipids, DNA, and DNA–Lipid Complexes

Rudolf Podgornik
National Institute of Child Health and Human Development, National Institutes of Health, Bethesda, Maryland, U.S.A., and University of Ljubljana, Ljubljana, Slovenia

D. Harries and V. A. Parsegian
National Institute of Child Health and Human Development, National Institutes of Health Bethesda, Maryland, U.S.A.

H. H. Strey
University of Massachusetts, Amherst Amherst, Massachusetts, U.S.A.

I. INTRODUCTION

Designed by nature for information and valued by molecular biologists for manipulation, DNA is also a favorite of physical chemists and physicists (1). Its mechanical properties (2), its interactions with other molecules (3), and its modes of packing (4) present tractable but challenging problems whose answers have in vivo and in vitro consequences. In the context of DNA transfection and gene therapy (5), what has been learned about molecular mechanics, interaction, and packing might teach us how to package DNA for more effective gene transfer. Among these modes of in vitro packaging are association with proteins, treatment with natural or synthetic cationic ''condensing agents,'' and combination with synthetic positively charged lipids (6).

In vivo, DNA is tightly held, not at all like the dilute solution form often studied in vitro (Fig. 1). This tight assembly necessarily incurs huge energetic costs of confinement, costs that create a tension under which DNA is expected to ravel or unravel its message. Through direct measurement of forces between DNA molecules (7) and direct observation of its modes of packing (8), we might see not only how to use concomitant energies to design better DNA transfer systems, but also how to better understand the sequences of events by which DNA is read in cells.

What binds these structures? To first approximation, for large, flexible biological macromolecules, the relevant interactions resemble those found among colloidal particles (9), where the size of the molecule (e.g., DNA molecules, lipid membranes, actin bundles) distinguishes it from simpler, smaller species (e.g., small solutes or salt ions). On the colloidal scale of tens of nanometers [1 nm = 10^{-9}m], only the interactions between macromolecules are evaluated explicitly, whereas the small molecular species only ''dress'' the large molecules and drive the interactions between them.

The electrical charge patterns of multivalent ions such as Mn^{+2}, Co^{3+}, or spermine^{+4} cation binding to negative DNA create attractive electrostatic and/or solvation forces that move DNA double helices to finite separations, despite the steric knock of DNA thermal Brownian motion (10). Solvation patterns about the cation-dressed structures create solvation forces: DNA–DNA repulsion because of water clinging to the surface, and attraction from the release of solvent (11). Positively charged histones will spool DNA into carefully distributed skeins, themselves arrayed for systematic unraveling and reading (12). Viral capsids will encase DNA, stuffed against its own DNA–DNA electrostatic and solvation repulsion, to keep it under pressure for release upon infection (13). In artificial preparations, the glue of positively charged and

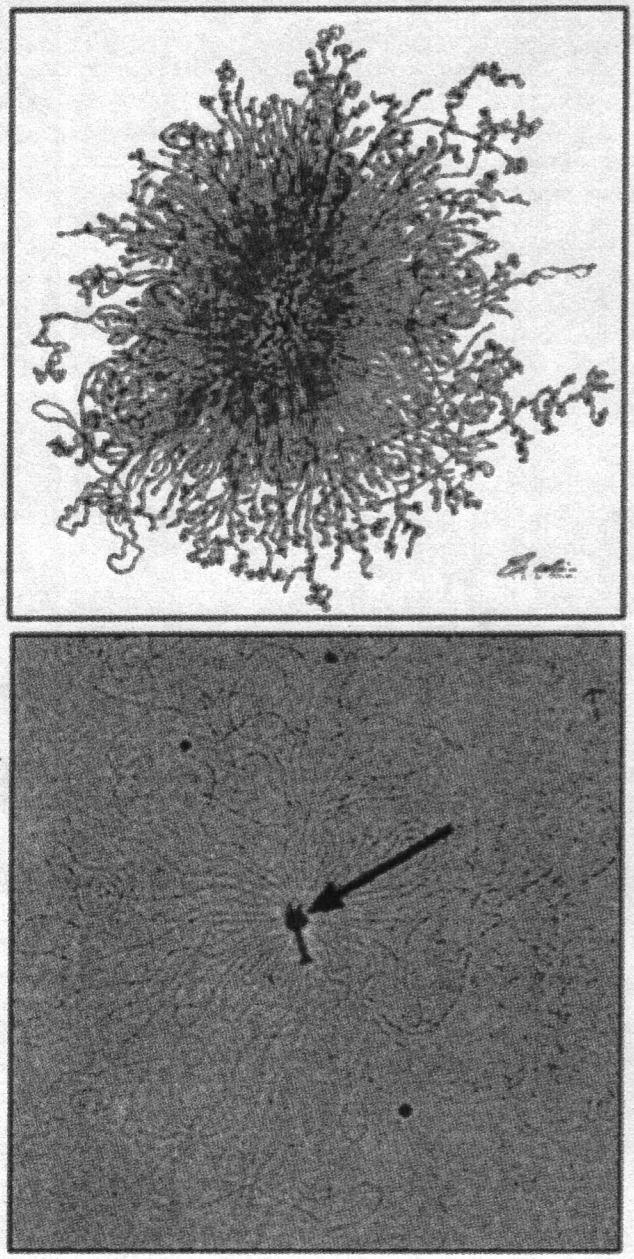

Figure 1 In vivo DNA is highly compacted. The figure shows *E. coli* DNA and T2 bacteriophage DNA after an osmotic shock in distilled water that has allowed them to expand from their much more compacted in vivo configurations. (*E. coli* picture courtesy of Ruth Kavenoff, Bluegenes, Inc., Los Angeles (1994); T2 picture from Kleinschmidt et al. BBA **61** (1962) 252.)

neutral lipids can lump negative DNA into ordered structures that can move through lipids and water solutions (14).

Changes in the suspending medium can modulate intermolecular forces. One example is the change in van der Waals charge fluctuation forces (see below) between lipid bilayers when small sugars modifying the dielectric dispersion properties of water are added to the solution (15). More dramatic, the addition of salt to water can substantially reduce electrostatic interactions between charged molecules such as DNA or other charged macromolecules bathed by an aqueous solution (16). These changes can modify the behavior of macromolecules quantitatively or induce qualitatively new features into their repertoire among these, most notably, precipitation of DNA by addition of organic polycations to the solution (10).

Similar observations can be made about the small molecules essential to practically every aspect of interaction between macromolecules. Through the dielectric constant or dielectric permittivity, it enters electrostatic interactions; through pH, it enters charging equilibria; and through its fundamental molecular geometry, it enters the hydrogen bond network topology around simple solutes. This is, of course, the water molecule (17). In what follows, we limit ourselves to only three basic properties of macromolecules—charge, polarity (solubility), and conformational flexibility—that appear to govern the plethora of forces encountered in biological milieu. It is no surprise that the highly ordered biological structures, such as the quasicrystalline spooling of DNA in viral heads or the multilamellar stacking of lipid membranes in visual receptor cells (Fig. 2), can be explained through the properties of a small number of fundamental forces acting between macromolecules. Detailed experimental as well as theoretical investigations have identified hydration, electrostatic, van der Waals or dispersion, and conformational fluctuation forces as the most fundamental interactions governing the fate of biological macromolecules.

Our intent here is to sketch the measurements of these operative forces and to dwell on concepts that rationalize them. It is from these concepts, with their insight into what controls organizing forces, that we expect people to learn to manipulate and package DNA in more rewarding ways.

II. MOLECULAR FORCES

A. The Origin and Measurement of Molecular Forces

We divide these forces into two broad categories, both of which can be either attractive or repulsive. First, there are interactions that are connected with fields emanating from sources within or on the macromolecules themselves (16) (e.g., electrostatic fields pointing from the fixed-charge distributions on macromolecules into the surrounding space, fields of connectivity of hydrogen bond networks extending from the macromolecular surfaces into the bulk solution that are seen in hydration interactions). Second, there are forces due to fluctuations that originate either in thermal Brownian motion or quantum jitter (15). Consequent interactions include the van der Waals or dispersion forces that originate from

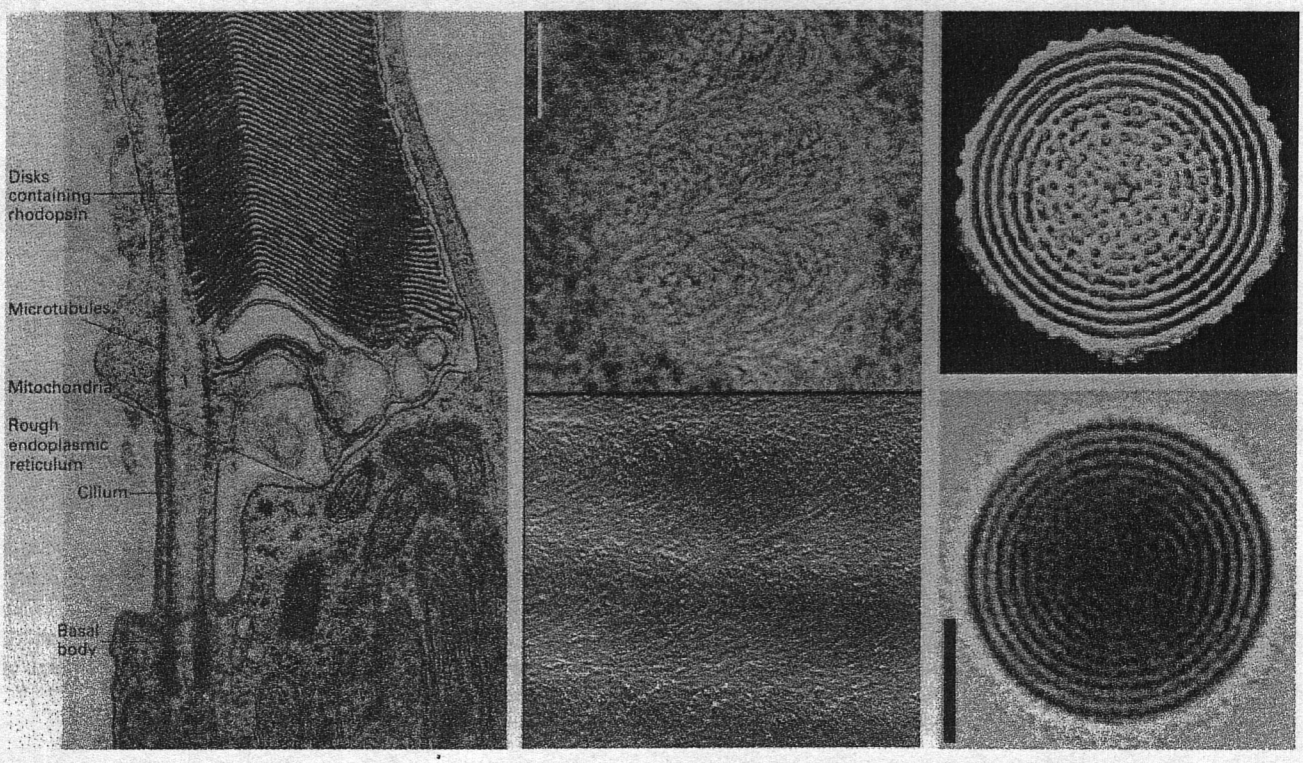

Figure 2 Highly ordered assemblies, ubiquitous among biological structures, can be explained through the properties of a very small number of fundamental forces acting between macromolecules. On the left-hand side, electron micrograph of a part of a human eye rod cell showing multilamellar bilayer aggregate. (From Kessel RG, Kardon RH. Tissues and Organs. San Francisco: W.H. Freeman and Co, 1979.) In the middle, electron micrograph of an in vivo cholesteric phase of a wild-type *E. coli* DNA. (Adapted from D. Frankiel–Krispin et al. EMBO J **20** (2001) 1184–1191.) For comparison we show the same type of structure for DNA in vitro below. (Adapted from A. Leforestier and F. Livolant, Biophys. J **65** (1993) 56–72.) On the right-hand side, cryomicrographs and computer-processed images of T7 phage heads showing ordered DNA spooling within the viral heads. (From Ref. 13.)

thermal as well as quantum mechanical fluctuations of electromagnetic fields in the space between and within the interacting molecules; conformation-fluctuation forces from thermal gyrations by the macromolecule when thermal agitation pushes against the elastic energy resistance of the molecule and confinement imposed by neighboring macromolecules (16).

There are many ways to detect interactions between macromolecules. Here we consider only macromolecules interacting in ordered arrays that are particularly relevant for investigations of the packing and energetics of DNA–lipid complexes.

A fundamental concept in macromolecular arrays is that of osmotic pressure (Fig. 3). It is equal to the pressure needed to hold a macromolecular array together against the forces acting between its constituent macromolecules. It can be applied either mechanically across a semipermeable membrane or via the osmotic stress of a high molecular weight (e.g., PEG (polyethyleneglycol), PVP (polyvinylpyrrolidone), dextrane) polymer solution. At chemical equilibrium, the osmotic pressure of one solution (macromolecular array) balances that of another (the bathing polymer solution). The chemical equilibrium can be maintained either via a semipermeable membrane or simply because the bathing polymer solution phase separates from the macromolecular array, as is many times the case with PEGs, PVP, and dextrane. This osmotical balancing of different molecular solutions is the basis of the ''osmotic stress method'' of measuring the equation of state of macromolecular arrays (18).

The equation of state of a macromolecular solution is defined as the dependence of its osmotic pressure on the density of the array (Fig. 4). By equilibrating the macromolecular array vs. a solution of high molecular weight polymer with a known osmotic pressure, one can set the osmotic pressure in the macromolecular array itself (18). If in addition the concurrent density of the macromolecular array is measured, either via X-ray scattering or direct densitometry, one gets the dependence of the osmotic pressure of the array on its density (i.e., its equation of state). This is the essence of the osmotic stress method.

1. Hydration Force

The hydration force is connected with a simple observation that it takes increasing amounts of work to remove water from

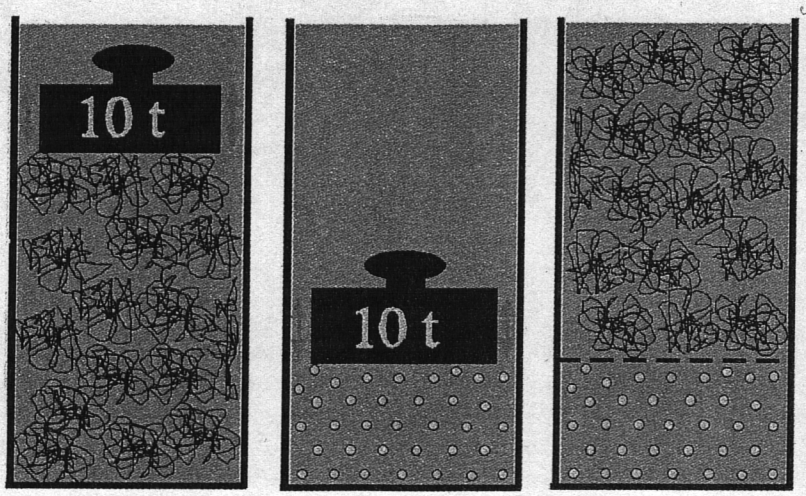

Figure 3 Osmotic pressure in macromolecular arrays. Dissolved polymers such as PEG exert an osmotic pressure on the the part of the solution from which they are excluded (shown schematically by the weight). Instead of exerting directly a pressure on the macromolecular subphase such as DNA or lipid arrays (small circles), one can equilibrate it with a solution of PEG at a set concentration (what amounts to the same thing: a set osmotic pressure) and PEG itself will exert osmotic stress on the macromolecular subphase. Osmotic weighing of polymers one against the other (the one with the known, set osmotic pressure against the unknown one) is the essence of the osmotic stress technique of measuring interactions in macromolecular solutions. See the color insert for a color version of this figure.

between electrically neutral lipids in multilamellar arrays, or from between ordered arrays of polymers at large polymer concentrations (18). Direct measurements of this work strongly suggest that it increases exponentially with the diminishing separation between colloid surfaces with a certain decay length that depends as much on the bulk properties of the solvent as on the detailed characteristics of the interacting surfaces. There is nevertheless some profound universality in the interactions between macromolecular surfaces at close distances (Fig. 5), whether they are charged, zwitterionic, or uncharged, that strongly suggest that water is essential in maintaining the stability of biological matter at high densities.

Hydration forces can be understood in different terms with no consensus yet on mechanism (11). Marčelja and coworkers (19) first proposed the idea that colloid surfaces perturb the vicinal water and that the exponential decay of the hydration force is due to the weakening of the perturbation of the solvent as a function of the distance between the interacting surfaces (Fig. 6). They introduced an order parameter $P(z)$ as a function of the transverse coordinate z, between the surfaces located at $z = D/2$ and $z = -D/2$, that would capture the local condition, or local ordering of solvent molecules between the surfaces. The detailed physical nature of this order parameter is left unspecified, but because the theory builds on general principles of symmetry and perturbation expansions molecular details are not needed. All one needs to know about P is that within the bulk water $P = 0$ and close to a macromolecular surface P remains nonzero. As a mnemonic, one can envision P as an arrow associated with each water molecule. In the bulk, the arrows point in all directions with equal probability. Close to a bounding macromolecular surface, they point preferentially toward or away from the surface (Fig. 6), depending on the surface-orienting fields.

If we envisage solvent molecules between two perturbing surfaces, we can decompose the total free energy F of their configuration into its energy W and entropy S parts via the well-known thermodynamic definition $F = W - TS$, where T is the temperature. Energetically it would be most favorable for the surface-induced order to persist away from the surfaces, but that would create conflict between the apposing surfaces (Fig. 3). Entropy fights any type of ordering and wants to eliminate all orderly configurations between the two surfaces, creating a homogeneous state of molecular disorder characterized by $P = 0$. Energy and entropy compromise to create a nonuniform profile of the order parameter between the surfaces; surface-induced order propagates but progressively decreases away from the surfaces.

From the free energy, we can derive the repulsive hydration osmotic pressure p acting between the surfaces because by definition it is proportional to the derivative of the free energy with respect to the separation D. Osmotic pressure between two apposed lipid surfaces has been measured extensively for different lipids (20) and has been measured to have the form $p = p_0 \exp(-D/\lambda_H)$, consistent with previously theoretically derived form of the hydration free energy if one assumes that $p_0 \sim P^2(z = D/2)$. Here λ_H is the hydration decay length of 0.1–0.4 nm measuring the spatial extent of water perturbation. From these experiments, one can deduce the magnitude of the prefactor p_0, which for a great variety of lipids and lipid mixtures can be found within an interval 10^{12} to 10^{10} dynes/cm^2. This ratio also

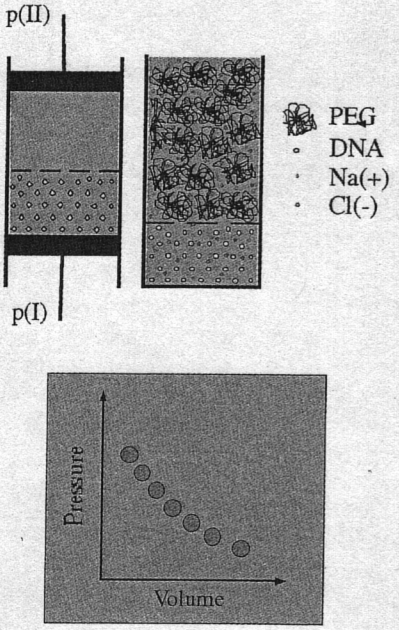

Figure 4 The osmotic stress method (18). DNA liquid crystals are equilibrated against solutions of a neutral polymer (e.g., PEG or PVP, depicted as disordered coils). These solutions are of known osmotic pressure, pH, temperature and ionic composition (54). Equilibration of DNA under the osmotic stress of external polymer solution is effectively the same as exerting mechanical pressure on the DNA subphase with a piston that passes water and small solutes but not DNA. After equilibration under this known stress, DNA separation is measured either by X-ray scattering, if the DNA subphase is sufficiently ordered, or by densitometry (55). DNA density and osmotic stress thus determined immediately provide an equation of state (osmotic pressure as a function of the density of the DNA subphase) to be codified in analytical form over an entire phase diagram. See the color insert for a color version of this figure.

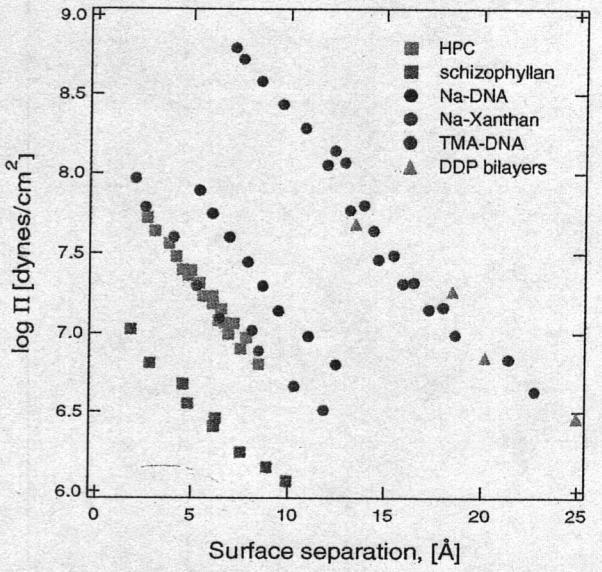

Figure 5 Interactions between biological macromolecules show pronounced universality at close surface-to-surface separations (or equivalently at very large densities). Hydroxypropyl cellulose, schizophillan, different DNA salts, xanthan, and DDP bilayers at small intermolecular separations (given in terms of the separation between effective molecular surfaces of the interacting molecules) all show strong repulsive interactions decaying with about the same characteristic decay length. The log-linear plot is thus more or less a straight line. (Composite data courtesy of D. C. Rau.) See the color insert for a color version of this figure.

determines the absolute magnitude of the hydration repulsion, which can be in the hundreds of atmospheres.

As already noted in this simple theoretical approach, the hydration decay length depends only on the bulk properties of the solvent, and not on the properties of the surface. To generalize this simplification, Kornyshev and Leikin (21) formulated a variant of the hydration force theory to also take into account explicitly the nature of surface ordering. They derive a modified hydration decay length that clearly shows how the surface order couples with the bare hydration decay length. Without going too deeply into this theory, we note that if the interacting surfaces have 2-dimensional ordering patterns characterized by a wave vector $Q = 2/\lambda$, where λ is the characteristic scale of the spatial variations of these patterns, then the effective hydration force decay length would be $\lambda_{KL} = \frac{1}{2} l_H (1 + 4^2(\lambda_H/\lambda)^2)^{-1/2}$. Inserting numbers for the case of DNA, where the "surface" structure has a characteristic scale of 1 to 2 Å, we realize that the hydration decay length in this case would be almost entirely determined by the surface structure and not the bulk solvent properties. Given the experimentally determined variety of forces between phospholipids (20), it is indeed quite possible that even in the simplest cases the measured decay lengths are not only those of the water solvent itself, but also include the surface properties via the characteristic scale of the surface ordering l_H.

The other important facet of this theory is that it predicts that in certain circumstances the hydration forces can become attractive (11). This is particularly important in the case of interacting DNA molecules where this hydration attraction connected with condensing agents can hold DNAs into an ordered array, even though the van der Waals forces themselves would be unable to accomplish that (22). This attraction is always an outcome of nonhomogeneous surface ordering and arises in situations where apposing surfaces have complementary checkerboard-like order (11). Unfortunately, in this situation, many mechanisms can contribute to attractions; therefore, it is difficult to argue for one strongest contribution.

2. Electrostatic Forces

Electrostatic forces between charged colloid bodies are among the key components of the force equilibria in (bio)colloid sys-

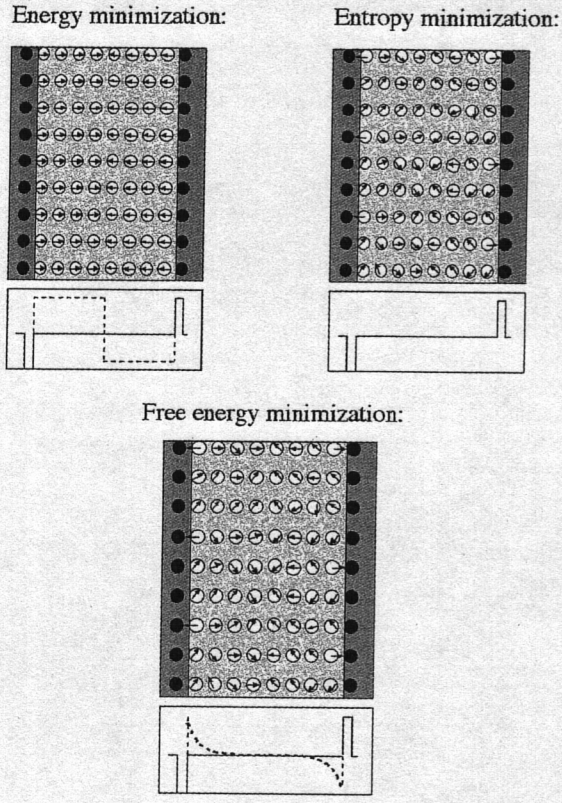

Figure 6 The hydration force. Marcelja and Radic (19) introduced an order parameter P that would capture the local condition, or local ordering, of solvent molecules between the surfaces. We represent it as an arrow (that has magnitude and direction) on each water molecule that is trapped between the two apposing surfaces and is being acted upon by the surface fields, depicted schematically with a bold line below each of the three drawings. Minimizing the energy corresponding to a spatial profile of P, leads to a configuration where P points (for example) away from both surfaces, and there is thus mismatch at the midplane (the dotted line below the leftmost drawing). The entropy would favor completely disordered configurations with no net value of P (the dotted line below the rightmost drawing). The free energy strikes a compromise between the two extrema, leading to a smooth profile of P, varying continuously as one goes from one surface to the other (the dotted line below the bottom drawing). As the two surfaces approach the nonmonotonic profile of the order parameter P leads to repulsive forces between them. See the color insert for a color version of this figure.

tems (23). At larger separations, they are the only forces that can counteract van der Waals attractions and thus stabilize colloid assembly. The crucial role of the electrostatic interactions in (bio)colloid systems is well documented and explored, following the seminal realization of Bernal and Fankuchen (24) that electrostatic interaction is the stabilizing force in tobacco mosaic virus (TMV) arrays.

Although the salient features of electrostatic interactions of fixed charges in a sea of mobile countercharges and salt ions are intuitively straightforward to understand, they are difficult to evaluate. These difficulties are clearly displayed by the early ambiguities in the sign of electrostatic interactions between two equally charged bodies that were first claimed to be attractive (Levine), then repulsive (Verwey-Overbeek), and finally that they were usually repulsive except if the counterions or the salt ions are of higher valency (25).

Here we introduce the electrostatic interaction on an intuitive footing (Fig. 7). Assume we have two equally charged bodies with counterions in-between. Clearly the minimum of electrostatic energy W_E (28), which for the electrostatic field configuration at the spatial position r, $E(r)$, is proportional to the integral of $E^2(r)$ over the whole space where one has nonzero electrostatic field, would correspond to adsorption of counterions to the charges leading to their complete neutralization. The equilibrium electrostatic field would thus be entirely concentrated next to the surface. However, at finite temperatures, it is not the electrostatic energy but rather the free energy (26), $F = W_E - TS$, also containing the entropy S of the counterion distribution, that should be minimized. The entropy of the mobile particles with the local density $\rho_i(r)$ [we assume there are more than 1 species of mobile particles, (e.g., counterions and salt ions) tracked through the index i] is taken as an ideal gas entropy (26), which is proportional to the volume integral of $\Sigma_i[\rho_i(r)\ln(\rho_i(r)/_{i0}) - (\rho_i(r)\text{-}\rho_{i0})]$, where ρ_{i0} is the density of the mobile charges in a reservoir that is in chemical equilibrium with the confined system under investigation. Entropy by itself would clearly lead to a uniform distribution of counterions between the charged bodies, $\rho_i(r) = \rho_{i0}$, whereas together with the electrostatic energy it obviously leads to a nonmonotonic profile of the mobile charge distribution between the surfaces, minimizing the total free energy of the mobile ions.

The above discussion, although far from being rigorous, contains the important theoretical underpinnings known as the Poisson–Boltzmann theory (27). To arrive at the central equation corresponding to the core of this theory, one simply has to formally minimize the free energy $F = W_E - TS$, just as in the case of structural interactions, together with the basic electrostatic equation (28) (the Poisson equation) that connects the sources of the electrostatic field with the charge densities of different ionic species. The standard procedure is now to minimize the free energy, take into account the Poisson equation, and what follows is the well-known Poisson–Boltzmann equation, the solution of which gives the nonuniform profile of the mobile charges between the surfaces with fixed charges. This equation can be solved explicitly for some particularly simple geometries (27). For two charged planar surfaces, the solution gives a screened electrostatic potential that decays exponentially away from the walls. It is thus smallest in the middle of the region between the surfaces and largest at the surfaces. The spatial variation of the electrostatic interaction is just as in the case of structural interactions described with a characteristic decay length, dubbed the Debye length in this case, which for uni-uni valent salts assumes the value

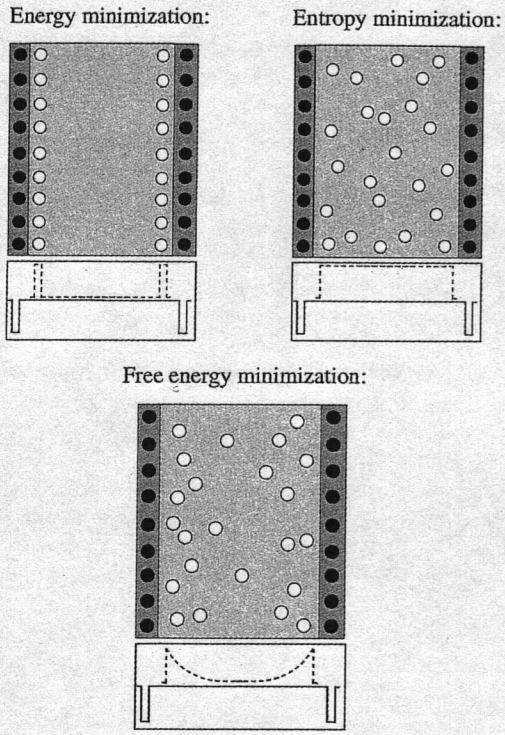

Figure 7 A pictorial exposition of the main ideas behind the Poisson–Boltzmann theory of electrostatic interactions between (bio)colloidal surfaces. Electrostatic energy by itself would favor adsorption of counterions (white circles) to the oppositely charged surfaces (black circles). The equilibrium profile of the counterions in this case is presented by the dotted line below the leftmost drawing. Entropy, to the contrary, favors a completely disordered configuration (i.e., a uniform distribution of counterions between the surfaces), presented by the dotted line below the rightmost drawing. The free energy works a compromise between the two principles leading to a nonmonotonic profile of the counterion density (25), varying smoothly in the intersurface region. As the two surfaces are brought close, the overlapping counterion distributions originating at the fixed charge at the surfaces (the bold line below each drawing) create repulsive forces between them. See the color insert for a color version of this figure.

of $\lambda_D = 3$ Å$/\sqrt{I}$, where I is the ionic strength of the salt in moles per liter. A 0.1 molar solution of uni-uni valent salt, such as NaCl, would thus have the characteristic decay length of about 9.5 Å. Beyond this separation, the charged bodies no longer feel each other. By adding or removing salt from the bathing solution, we are thus able to regulate the range of electrostatic interactions.

The exponential decay of the electrostatic field away from the charged surfaces with a characteristic length, independent (to the lowest order) of the surface charge, is one of the most important results of the Poisson–Boltzmann theory.

Obviously, as the surfaces come closer together, their decaying electrostatic potentials begin to interpenetrate (25). The consequence of this interpenetration is a repulsive force between the surfaces that again decays exponentially with the intersurface separation and a characteristic length again equal to the Debye length. For two planar surfaces at a separation D, bearing sufficiently small charges, characterized by the surface charge density σ, so that the ensuing electrostatic potential is never larger than k_BT/e, where k_B is Boltzmann's constant and e is the elementary electron charge, one can derive (27) for the interaction free energy per unit surface area $F(D)$ the expression $F(D) \sim \sigma^2 \exp(-D/\lambda_D)$. Obviously the typical magnitude of the electrostatic interaction in different systems depends on the magnitude of the surface charge. It would not be unusual in lipids to have surface charge densities in the range of 1 elementary charge per 50 to 100 Å^2 surface area (29). For this range of surface charge densitities, the constant prefactor in the expression for the osmotic pressure would be of the order 0.4 to 1.2 $\times$ 10^7 N/m.

The same type of analysis would also apply to two charged cylindrical bodies (e.g., two molecules of DNA) interacting across an electrolyte solution. What one evaluates in this case is the interaction free energy per unit length of the cylinders (30), $g(R)$, where R is the separation between the cylinders that can be obtained in the approximate form $g(R) \sim \mu^2 \exp(-R/\lambda_D)$. It is actually possible to also get an explicit form (30) of the interaction energy between two cylinders even if they are skewed by an angle θ between them. In this case, the relevant quantity is the interaction free energy itself (if θ is nonzero, then the interaction energy does not scale with the length of the molecules) that can be obtained in a closed form as $F(R,\theta) \sim \mu^2 \lambda_D R^{1/2} \exp(-R/\lambda_D)/\sin(\theta)$.

The predictions for the forces between charged colloid bodies have been reasonably well borne out for electrolyte solutions of uni-uni valent salts (31). In that case, there is near quantitative agreement between theory and experiment. However, for higher valency salts, the Poisson–Boltzmann theory does not only give the wrong numerical values for the strength of the electrostatic interactions, but also misses their sign. In higher valency salts, the correlations among mobile charges between charged colloid bodies due to thermal fluctuations in their mean concentration lead effectively to attractive interactions (32) that are in many respects similar to the van der Waals forces that are analyzed next.

3. van der Waals Forces

van der Waals charge fluctuation forces are special in the sense that they are a consequence of thermodynamic and quantum mechanical fluctuations of the electromagnetic fields (15). They exist even if the average charge, dipole moment, or higher multipole moments on the colloid bodies are zero. This is in stark contrast to electrostatic forces that require a net charge or a net polarization to drive the interaction. This also signifies that the van der Waals forces are much more general and ubiquitous than any other force between colloid bodies (9).

There are many different approaches to the van der Waals forces (15,33). For interacting molecules, one can distinguish different contributions to the van der Waals force, stemming from thermally averaged dipole–dipole potentials (the Keesom interaction), dipole-induced dipole interactions (the Debye interaction), and induced dipole-induced dipole interactions (the London interaction) (34). They are all attractive and their respective interaction energy decays as the sixth power of the separation between the interacting molecules. The magnitude of the interaction energy depends on the electromagnetic absorption (dispersion) spectrum of interacting bodies, thus also the term dispersion forces.

For large colloidal bodies composed of many molecules, the calculation of the total van der Waals interactions is no trivial matter (15), even if we know the interactions between individual molecules composing the bodies. Hamaker assumed that one can simply add the interactions between composing molecules in a pairwise manner. It turned out that this was a very crude and simplistic approach to van der Waals forces in colloidal systems because it does not take into account the highly nonlinear nature of the van der Waals interactions in condensed media. Molecules in a condensed body interact among themselves, thus changing their properties (c.f. their dispersion spectrum) that in their turn modify the van der Waals forces between them.

Lifshitz, following work of Casimir (9,15), realized how to circumvent this difficulty and formulated the theory of van der Waals forces in a way that already includes all these nonlinearities. The main assumption of this theory is that the presence of dielectric discontinuities as in colloid surfaces, modifies the spectrum of electromagnetic field modes between these surfaces (Fig. 8). As the separation between colloid bodies varies, so do the eigenmode frequencies of the electromagnetic field between and within the colloid bodies. It is possible to deduce the change in the free energy of the electromagnetic modes due to the changes in the separation between colloid bodies coupled to their dispersion spectral characteristics (35).

Based on the work of Lifshitz, it is now clear that the van der Waals interaction energy is just the change of the free energy of field harmonic oscillators at a particular eigenmode frequency ω as a function of the separation between the interacting bodies D and temperature T, $\omega = \omega(D,T)$. With this equivalence in mind, it is quite straightforward to calculate the van der Waals interaction free energy between two planar surfaces at a separation D and temperature T; the dielectric permittivity between the two surfaces, ε and within the surfaces, ε', must both be known as a function of the frequency of the electromagnetic field (35). This is a consequence of the fact that, in general, the dielectric media comprising the surfaces as well as the space between them are dispersive, meaning that their dielectric permittivities depend on frequency of the electromagnetic field [i.e., $\varepsilon = \varepsilon(\omega)$]. With this in mind one can derive the interaction free energy per unit surface area of the interacting surfaces in the form $F(D) = A/12\pi D^2$, where the s.c. Hamaker coefficient A depends on the difference between the dielectric permittivities of the interacting materials at different imaginary frequencies. It can be in general split into two terms: the first term in the Hamaker coefficient is due to thermodynamic fluctuations, such as Brownian rotations of the dipoles of the molecules composing the media or the averaged dipole-induced dipole forces and depends on the static ($\omega = 0$) dielectric response of the interacting media, whereas the second term is purely quantum mechanical in nature (15). The imaginary argument of the dielectric constants is not that odd because $\varepsilon(\iota\zeta)$ is an even function of ζ, which makes $\varepsilon(\iota\zeta)$ also a purely real quantity (35).

To evaluate the magnitude of the van der Waals forces, one thus has to know the dielectric dispersion $\varepsilon(\omega)$ of all the media involved. This is no simple task and can be accomplished only for very few materials (34). Experiments seem to be a much more straightforward way to proceed. The values for the Hamaker coefficients of different materials interacting

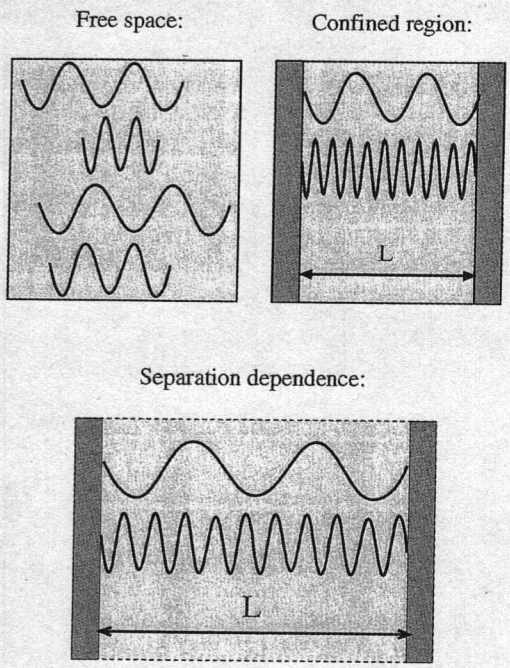

Figure 8 A pictorial introduction to the theory of Lifshitz–van der Waals forces between colloid bodies. Empty space is alive with electromagnetic (EM) field modes that are excited by thermal as well as quantum mechanical fluctuations. Their frequency is unconstrained and follows the black body radiation law. Between dielectric bodies, only those EM modes survive that can fit into a confined geometry. As the width of the space between the bodies varies, so do the allowed EM mode frequencies. Every mode can be treated as a separate harmonic oscillator, each contributing to the free energy of the system. Because this free energy depends on the frequency of the modes, that in turn depend on the separation between the bodies, the total free energy of the EM modes depends on the separation between the bodies. This is an intuitive description of the Lifshitz–van der Waals force (15). See the color insert for a color version of this figure.

across water are between 0.3 and 2.0 $\times$ 10^{-20} J. Specifically for lipids, the Hamaker constants are quite close to theoretical expectations except for the phosphatidylethanolamines that show much larger attractive interactions probably due to headgroup alignment (31). Evidence from direct measurements of attractive contact energies as well as direct force measurements suggest that van der Waals forces are more than adequate to provide attraction between bilayers for them to form multilamellar systems (36).

For cylinders the same type of argument applies, except that due to the geometry the calculations are a bit more tedious (37). Here the relevant quantity is not the free energy per unit area but the interaction free energy per unit length of the two cylinders of radius a, $g(R)$, considered to be parallel at a separation R. The calculation (38) leads to the following form $g(R) \sim A\ a^4/R^5$, where the constant A again depends on the differences between dielectric permittivities $\varepsilon_{\|}$, the parallel, and $\varepsilon_{\perp}$, the perpendicular components of the dielectric permittivity of the dielectric material of the cylinders, and ε_m, the dielectric permittivity of the bathing medium.

If, however, the 2 interacting cylinders are skewed, then the interaction free energy $G(R, \theta)$, this time not per length, is obtained (38) in the form $G(R) \sim (A + B\cos^2\theta)(a^4/R^4\sin\theta.)$ The constants A and B describe the dielectric mismatch between the cylinder and the bathing medium at different imaginary frequencies. The same correspondence between the thermodynamic and quantum mechanical parts of the interactions as for two parallel cylinders also applies to this case. Clearly, the van der Waals force between two cylinders has a profound angular dependence that in general creates torques between the two interacting molecules.

Taking the numerical values of the dielectric permittivities for two interacting DNA molecules, one can calculate that the van der Waals forces are quite small, typically 1 to 2 orders of magnitude smaller than the electrostatic repulsions between them, and in general cannot hold the DNAs together in an ordered array. Other forces, leading to condensation phenomena in DNA (10) clearly have to be added to the total force balance in order to get a stable array. There is as yet still no consensus on the exact nature of these additional attractions. It seems that they are due to the fluctuations of counterion atmosphere close to the molecules.

4. The DLVO Model

The popular Derjaguin-Landau-Verwey-Overbeek (DLVO) (9,25) model assumes that electrostatic double-layer and van der Waals interactions govern colloid stability. Applied with a piety not anticipated by its founders, this model actually does work rather well in surprisingly many cases. Direct osmotic stress measurements of forces between lipid bilayers show that at separations less than ~10 Å there are qualitative deviations from DLVO thinking (39). For micron-size objects and for macromolecules at greater separations, electrostatic double-layer forces and sometimes van der Waals forces tell us what we need to know about interactions governing movement and packing.

5. Geometric Effects

Forces between macromolecular surfaces are most easily analyzed in plane parallel geometry. Because most of the interacting colloid surfaces are not planar, one has either to evaluate molecular interactions for each particular geometry or to devise a way to connect the forces between planar surfaces with forces between surfaces of a more general shape. The Derjaguin approximation (9) assumes that interactions between curved bodies can be decomposed into interactions between small plane-parallel sections of the curved bodies (Fig. 9). The total interaction between curved bodies would be thus equal to a sum where each term corresponds to a partial interaction between quasi-plane-parallel sections of the two bodies. This idea can be given a completely rigorous form and leads to a connection between the interaction free energy per unit area of two interacting planar surfaces, $F(D)$, and the force acting between two spheres at minimal separation D, $f(D)$, 1 with the mean radius of curvature R_1 and the other 1 with R_2. The formal equivalence can be written as follows, $f(D) = 2\pi (R_1R_2/(R_1+R_2))\ F(D)$. A similar equation can also be obtained for 2 cylinders in the form, $f(D) = 2\pi(R_1R_2)^{1/2}\ F(D)$.

These approximate relations clearly make the problem of calculating interactions between bodies of general shape tractable. The only caveat here is that the radii of curvature should be much larger than the proximal separation between the two interacting bodies, effectively limiting the Derjaguin approximation to sufficiently small separations.

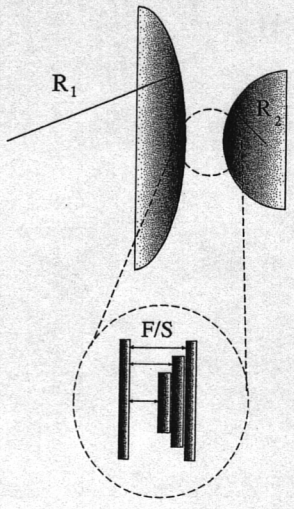

Figure 9 The Derjaguin approximation. To formulate forces between oppositely curved bodies (e.g., cylinders, spheres, etc.) is very difficult, but it is often possible to use an approximate procedure. Two curved bodies (two spheres of unequal radii in this case) are approximated by a succession of planar sections, interactions between which can be calculated relatively easy. The total interaction between curved bodies is obtained through a summation over these planar sections.

Using the Derjaguin formula or evaluating the interaction energy explicitly for those geometries for which this indeed is not an insurmountable task, one can now obtain a whole zoo of DLVO expressions for different interaction geometries (Fig. 10). The salient features of all these expressions are that the total interaction free energy always has a primary minimum, that can only be eliminated by strong short-range hydration forces, and a secondary minimum due to the compensation of screened electrostatic repulsion and van der Waals–Lifshitz attraction. The position of the secondary minimum depends as much on the parameters of the forces (Hamaker constant, fixed charges, and ionic strength) as on the interaction geometry. Generally, the range of interaction between the bodies of different shapes is inversely proportional to their radii of curvature.

Thus, the longest-range forces are observed between planar bodies, and the shortest between small (pointlike) bodies.

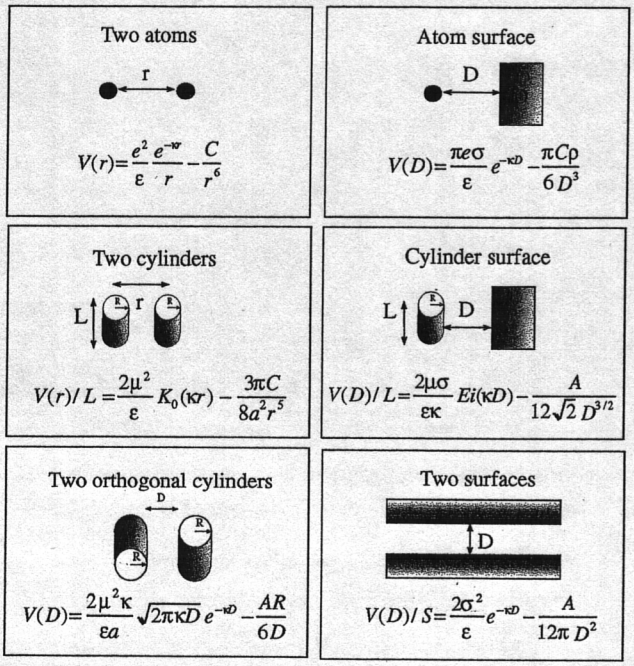

Figure 10 A menagerie of DLVO interaction expressions for different geometries most commonly encountered in biological milieu. Two small particles, a particle and a wall, 2 parallel cylinders, a cylinder close to a wall, 2 skewed cylinders and 2 walls. The DLVO interaction free energy is always composed of a repulsive electrostatic part (calculated from a linearized Poisson–Boltzmann theory) and an attractive van der Waals part. Charge: e, charge per unit length of a cylinder: μ, charge per unit surface area of a wall: σ, C is a geometry-dependent constant, ε the dielectric constant, κ the inverse Debye length, and ρ the density of the wall material. The functions $K_0(x)$ (the Bessel function K_0) and $Ei(x)$ (the exponential integral function) both depend essentially exponentially on their respective argument.

What we have not indicated in Fig. 7 is that the interaction energy between two cylindrical bodies, skewed at a general angle θ and not just for parallel or crossed configurations, can be obtained in an explicit form. It follows simply from these results that the configuration of two interacting rods with minimal interaction energy is the one corresponding to $\theta = \pi/2$ (i.e., corresponding to crossed rods).

6. Fluctuation Forces

The term ''fluctuation forces'' is a bit misleading in this context because clearly van der Waals forces are already fluctuation forces. What we have in mind is thus a generalization of the van der Waals forces to situations where the fluctuating quantities are not electromagnetic fields but other quantities subject to thermal fluctuations. No general observation as to the sign of these interactions can be made, they can be either repulsive or attractive and are as a rule of thumb comparable in magnitude to the van der Waals forces.

The most important and ubiquitous force in this category is the undulation or Helfrich force (41). It has a very simple origin and operates among any type of deformable bodies as long as their curvature moduli are small enough (comparable to thermal energies). It was shown to be important for multilamellar lipid arrays (41) as well as in hexagonal polyelectrolyte arrays (42) (Fig. 11).

The mechanism is simple. The shape of deformable bodies fluctuates because of thermal agitation (Brownian motion) (26). If the bodies are close to each other, the conformational fluctuations of one will be constrained by the fluctuations of its neighbors. Thermal motion makes the bodies bump into each other, which creates spikes of repulsive force between them. The average of this force is smooth and decays continuously with the mean separation between the bodies.

One can estimate this steric interaction for multilamellar lipid systems and for condensed arrays of cylindrical polymers (Fig. 11). The only quantity entering this calculation is the elastic energy of a single bilayer that can be written as the square of the average curvature of the surface, summed over the whole area of the surface, multiplied by the elastic modulus of the membrane, K_C. K_C is usually between 10 and 50 k_BT (43) for different lipid membranes. If the instantaneous deviation of the membrane from its overall planar shape in the plane is now introduced as u, the presence of neighboring membranes introduces a constraint on the fluctuations of u that basically demands, that the average of the square of u must be proportional to D^2, where D is the average separation between the membranes in a multilamellar stack. Thus, we should have $u^2 \sim D^2$. The free energy associated with this constraint can now be derived in the form (40) $F(D) \sim (k_BT)^2/(K_CD^2)$, and is seen to decay in inverse proportion to the separation between bilayers squared.

It has thus obviously the same dependence on D as the van der Waals force. This is, however, not a general feature of undulation interactions as the next example clearly shows. Also, we only indicated the general proportionality of the interaction energy. Calculation of the prefactors can be a difficult (44), especially because the elastic bodies usually do not

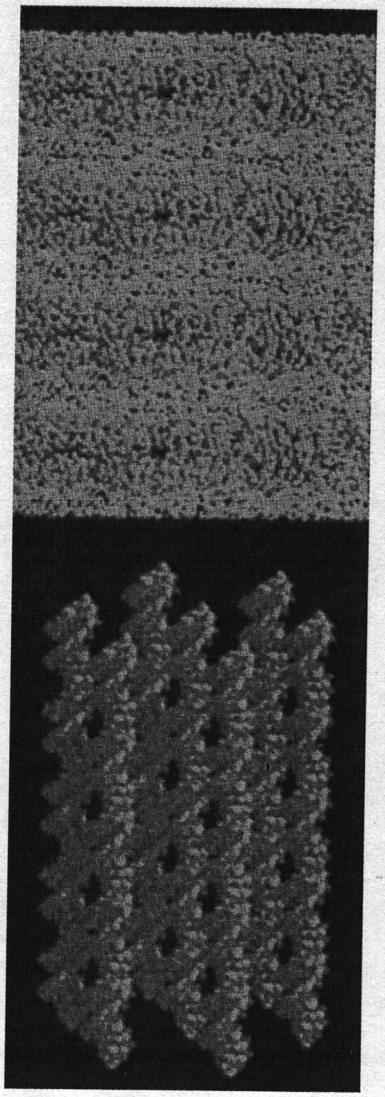

Figure 11 Thermally excited conformational fluctuations in a multilamellar membrane array (small molecules are waters and long-chain molecules are phospholipids) or in a tightly packed polyelectrolyte chain array (the figure represents a hexagonally packed DNA array) lead to collisions between membranes or polyelectrolyte chains. These collisions contribute an additional repulsive contribution to the total osmotic pressure in the array, a repulsion that depends on the average spacing between the fluctuating objects. See the color insert for a color version of this figure.

interact with idealized hard repulsions but rather through soft potentials that have both attractive as well as repulsive regimes.

The same line of thought can now be applied to flexible polymers in a condensed array (42). This system is a 1-dimensional analog of the multilamellar membrane system. For polymers, the elastic energy can be written similarly to the membrane case as the square of the local curvature of the polymer, multiplied by the elastic modulus of the polymer, integrated over its whole length. The elastic modulus K_c is usually expressed through a persistence length $L_p = K_c/(k_BT)$. The value of the persistence length tells us how long a polymer can be before the thermal motion forces it to fluctuate wildly. For DNA, this length is about 50 nm. However, it spans the whole range of values between about 10 nm for hyaluronic acid, all the way to 3 mm for microtubules. Using the same constraint for the average fluctuations of the polymer away from the straight axis, one derives for the free energy change due to this constraint the relationship $F(D) \sim (k_BT)/(L_p^{1/3}D^{2/3})$ (42).

Clearly, the D dependence for this geometry is much different from the one for van der Waals force, which would be D^{-5}. There is thus no general connection between the van der Waals force and the undulation fluctuation force. Here again, one has to indicate that if the interaction potential between fluctuating bodies is described by a soft potential, with no discernible hard core, the fluctuation interaction can have a profoundly different dependence on the mean separation (42).

Apart from the undulation fluctuation force, there are other fluctuation forces. The most important among them appears to be the monopolar charge fluctuation force (45), recently investigated in the context of DNA condensation. It arises from transient charge fluctuations along the DNA molecule due to constant statistical redistributions of the counterion atmosphere.

The theory of charge fluctuation forces is quite intricate and mathematically demanding (46). Let us just quote a rather interesting result, viz. if two point charges interact via a ''bare'' potential $V_0(R)$, where R is the separation between them, then the effect of the thermal fluctuations in the number of counterions surrounding these charges would lead to an effective interaction of the form $V(R) \sim -k_BTV_0^2(R)$. The fluctuation interaction in this case would thus be attractive and proportional to the square of the bare interaction.

This simple result already shows one of the salient features of the interaction potential for monopolar charge fluctuation forces, viz. it is screened with half the Debye screening length [because of $V_0^2(R)$]. If there is no screening, however, the monopolar charge fluctuation force becomes the strongest and longest ranged among all fluctuation forces. It is however much less general than the related van der Waals force, and it is still not clear what the detailed conditions should be for its appearance, the main difficulty being the question of whether charge fluctuations in the counterion atmosphere are constrained.

7. Lessons

Molecular forces apparently convey a variety that is surprising considering that they are all to some extent or another just a variant of electrostatic interactions. Quantum and thermal fluctuations apparently modify the underlying electrostatics, leading to qualitatively novel and unexpected features. The

zoo of forces obtained in this way is what one has to deal with and understand when trying to make them work for us.

III. DNA MESOPHASES

A. Polyelectrolyte Properties of DNA

We can define several levels of DNA organization similarly to (1). Its primary structure is the sequence of base pairs. Its secondary structure is the famous double helix that can exist in several conformations. In solution, the B-helical structure dominates (47). The bases are perpendicular to the axis of the molecule and are 0.34 nm apart, and 10 of them make 1 turn of the helix. These parameters can vary for DNA in solution where up to 10.5 base pairs can make a whole turn of the double helix (48). In the A structure, the bases are tilted with respect to the direction of the helix, and this arrangement yields an internal hole, wider diameter, and closer packing (Fig. 12). Other conformations, such as the left-handed Z form, are rare. In solution, DNA's tertiary structure includes the many bent and twisted conformations in 3 dimensions.

DNA lengths can reach macroscopic dimensions. For instance, the human genome is coded in approximately 3 billion base pairs with a collective linear stretch on the order of a meter. Obviously, this molecule must undergo extensive compaction in order to fit in the cell nucleus. In natural environments, DNA is packaged by basic proteins, which form chromatin structures to keep DNA organized. In the test tube, DNA can be packaged into very tight and dense structures as well, primarily by various "condensing" agents. Their addition typically induces a random coil to globule transition. At large concentrations, DNA molecules, like lipids, form ordered liquid crystalline phases (10) that have been studied extensively at different solution conditions (8).

In vitro, at concentrations above a critical value (49), polyelectrolyte DNA self-organizes in highly ordered mesophases (8). In this respect, it is a lyotropic liquid crystal. But contrary to the case of lipid mesophases, where the shape of constituent molecules plays a determining role, the organization of DNA in condensed phases is primarily a consequence of its relatively large stiffness (8). The orientational ordering of DNA at high concentrations is promoted mostly by the interplay between entropically favored disorder or misalignment and the consequent price in terms of the high interaction energy. The mechanism of orientational ordering is thus the same as in standard short nematogens (50). The main difference being due to the large length of polymeric chains. The discussion that follows concentrates mostly on very long, on the order of 1000 persistence lengths thus microns long, DNA molecules.

B. Flexibility of DNA Molecules in Solution

In isotropic solutions, DNA can be in one of several forms. For linear DNA, individual molecules are effectively straight over the span of a persistence length that can also be defined as the exponential decay length for the loss of angular correlation between 2 positions along the molecule, while for longer

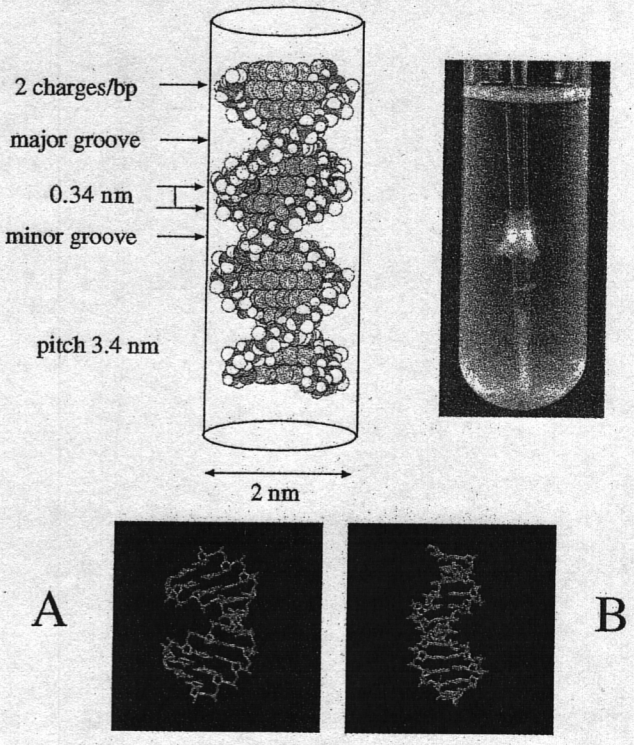

Polymer	Solvent	Persistence length [nm]
Microtubule	water	3000000
F-actin	water	15000
Schizophyllan	water	200
Xanthan	0.1 M NaCl	120
DNA	0.2 M NaCl	50
Hyaluronic acid	0.2 M NaCl	7

Figure 12 Structural parameters of a DNA molecule. The two relevant configurations of the DNA backbone: A-DNA, common at small hydrations or high DNA densities, and B-DNA common in solution at large hydrations and lower DNA densities. The test tube holds ethanol-precipitated DNA in solution. Its milky color is due to the light scattering by thermal conformational fluctuations in the hexatic phase (see main text). Box: typical persistence lengths for different (bio)polymer chains in nm. See the color insert for a color version of this figure.

lengths they form a wormlike random coil. The persistence length of DNA is about 50 nm (1). The persistence length has been determined by measuring the diffusion coefficient of different-length DNA molecules using dynamic light scattering and by enzymatic cyclization reactions (51). It depends only weakly on the base-pair sequence and ionic strength.

DNA can also be circular as in the case of a plasmid. The closed form of a plasmid introduces an additional topological constraint on the conformation that is given by the linking number Lk (2). The linking number gives the number of heli-

cal turns along a circular DNA molecule. Because plasmid DNA is closed, Lk has to be an integer number. By convention, Lk of a closed right-handed DNA helix is positive. The most frequent DNA conformation for plasmids in cells is negatively supercoiled. This means that for such plasmids Lk is less than it would be for a torsionally relaxed DNA circle—negatively supercoiled DNA is underwound. This is a general phenomenon with important biological consequences. It seems that free energy of negative supercoiling catalyzes processes that depend on DNA untwisting, such as DNA replication and transcription, which rely on DNA (52). Although the sequence of bases in exons determine the nature of proteins synthesized, it is possible that such structural features dictate the temporal and spatial evolution of DNA-encoded information.

C. Liquid Crystals

The fact that DNA is intrinsically stiff makes it form liquid crystals at high concentration (8). Known for about 100 years, the simplest liquid crystals are formed by rodlike molecules. Solutions of rods exhibit a transition from an isotropic phase with no preferential orientation to a nematic phase, a fluid in which the axes of all molecules point on average in 1 direction (Fig. 11). The unit vector in which the molecules point is called the nematic director n. Nematic order is orientational order (50), in contrast to positional order that distinguishes between fluid and crystalline phases. Polymers with intrinsic stiffness can also form liquid crystals. This is because a long polymer with persistence length L_p acts much like a solution of individual rods that are all one persistence length long, thus the term ''polymer nematics'' (53).

If the molecules that comprise the liquid crystal are chiral, have a natural twist such as double-helical DNA, then their orientational order tends to twist. This twist originates from the interaction between two molecules that are both of the same handedness. This chiral interaction is illustrated in Fig. 13 for two helical or screwlike molecules. For steric reasons, two helices pack best when tilted with respect to each other. Instead of a nematic phase chiral molecules form a cholesteric phase (50). The cholesteric phase is a twisted nematic phase in which the nematic director twists continuously around the so-called cholesteric axis as shown in Fig. 13. Using the same arguments as for plain polymers, chiral polymers will form polymer cholesterics.

Both cholesteric and hexagonal liquid crystalline DNA phases were identified in the 1960s. This discovery was especially exciting because both phases were also found in biological systems. The hexagonal liquid crystalline phase can be seen in bacterial phages, and the cholesteric phase can be seen in cell nuclei of dinoflagellates (8).

D. Measurements of Forces Between DNA Molecules

Liquid crystalline order lets us measure intermolecular forces directly. With the osmotic stress method, DNA liquid crystals

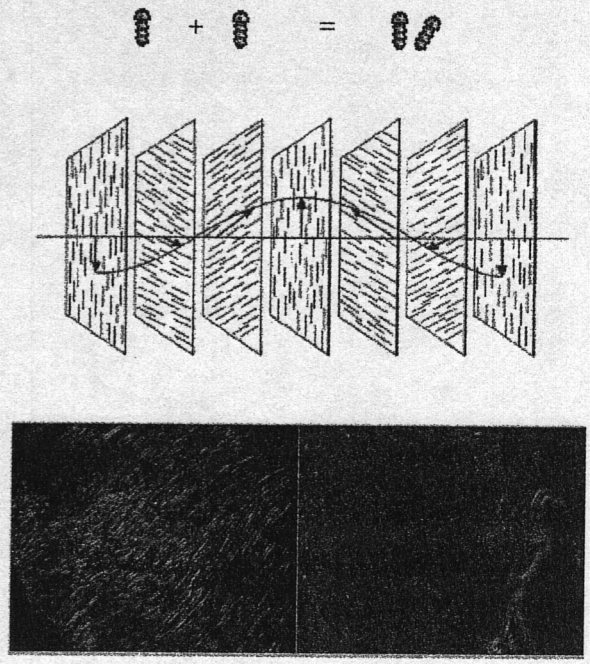

Figure 13 Chiral interaction for two helical or screwlike molecules. For steric reasons, two helices just as two screws (depicted on the figure) pack best when slightly tilted with respect to each other. Because of DNA's double-stranded, helical nature, it is a type of molecular screw and exhibits chiral interactions. Instead of a nematic phase depicted on Fig. 11, characterized by the average constant direction of molecules, chiral molecules form a cholesteric phase (50). The cholesteric phase is a twisted nematic phase in which the nematic director twists continuously around a ''cholesteric axis'' depicted on the middle drawing. Under crossed polarizers (bottom), the DNA cholesteric phase creates a characteristic striated texture. For long DNA molecules, the striations appear disordered.

are equilibrated against neutral polymer (e.g., PEG or PVP) solutions of known osmotic pressure, pH, temperature, and ionic composition (54). Equilibration of DNA under osmotic stress of external polymer solution is effectively the same as exerting mechanical pressure on the DNA subphase with a piston [see Fig. 4]. In this respect, the osmotic stress technique is formally much similar to the Boyle experiment where one compresses a gas with mechanical pistons and measures the ensuing pressure. After equilibration under this known stress, DNA separation is measured either by X-ray scattering, if the DNA subphase is sufficiently ordered, or by straightforward densitometry (55). Known DNA density and osmotic stress immediately provide an equation of state (osmotic pressure as a function of the density of the DNA subphase) to be codified in analytical form for the entire phase diagram. Then, with the local packing symmetry derived from X-ray scatter-

ing (7,54), and sometimes to correct for DNA motion (42), it is possible to extract the bare interaxial forces between molecules that can be compared with theoretical predictions as developed in Chapter 2. In vivo observation of DNA liquid crystals (56) shows that the amount of stress needed for compaction and liquid crystalline ordering is the same as for DNA in vitro.

E. Interactions Between DNA Molecules

Performed on DNA in univalent salt solutions, direct force measurements reveal two types of purely repulsive interactions between DNA double helices (4):

1. At interaxial separations less than ~3 nm (surface separation ~1 nm), an exponentially varying "hydration" repulsion believed to originate from partially ordered water near the DNA surface.
2. At surface separations greater than 1 nm, measured interactions reveal electrostatic double-layer repulsion, presumably from negative phosphates along the DNA backbone.

Measurements give no evidence for a significant DNA–DNA attraction expected on theoretical grounds (57). Although charge fluctuation forces must certainly occur, they appear to be negligible at least for liquid crystal formation in monovalent-ion solutions. At these larger separations, the double-layer repulsion often couples with configurational fluctuations to create exponentially decaying forces whose decay length is significantly larger than the expected Debye screening length (42).

Bare short-range molecular interactions between DNA molecules appear to be insensitive to the amount of added salt. This has been taken as evidence that they are not electrostatic in origin, as attested also by similar interactions between completely uncharged polymers such as schizophilline (Fig. 5). The term hydration force associates these forces with perturbations of the water structure around DNA surface (54). Alternatively, short-range repulsion has been viewed as a consequence of the electrostatic force specific to high DNA density and counterion concentration (58).

F. High-density DNA Mesophases

Ordering of DNA can be induced by two alternative mechanisms. First of all, attractive interactions between different DNA segments can be enhanced by adding multivalent counterions believed to promote either counterion correlation forces (59) or electrostatic (60) and hydration attraction (22). In these cases, DNA aggregates spontaneously. Alternatively, one can add neutral crowding polymers to the bathing solution that phase separate from DNA and exert osmotic stress on the DNA subphase (61). In this case the intersegment repulsions in DNA are simply counteracted by the large externally applied osmotic pressure. DNA is forced in this case to condense under externally imposed constraints. This latter case is formally (but only formally) analogous to a Boyle gas pressure experiment but with osmotic pressure playing the role of ordinary pressure. The main difference being that ordinary pressure is set mechanically, whereas osmotic pressure has to be set through the chemical potential of water, which is in turn controlled by the amount of neutral crowding polymers (e.g., PEG, PVP, dextran) in the bathing solution (55).

At very high DNA densities, where the osmotic pressure exceeds 160 atm, DNA can exist only in a (poly)crystalline state (62). Nearest neighbors in such an array are all oriented in parallel and show correlated (nucleotide) base stacking between neighboring duplexes (Figs. 11 and 14). This means that there is a long-range correlation in the positions of the backbone phosphates between different DNA molecules in the crystal. The local symmetry of the lattice is monoclinic. Because of the high osmotic pressure, DNA is actually forced to be in an A conformation characterized by a somewhat larger outer diameter as well as a somewhat smaller pitch than in the canonical B conformation (see Fig. 12), which persists at smaller densities. If the osmotic pressure of such a crystal is increased above 400 atm, the helix begins to crack and the sample loses structural homogeneity (62).

Lowering the osmotic pressure does not have a pronounced effect on the DNA crystal until it is down to ~160 atm. Then the crystal as a whole simultaneously expands while individual DNA molecules undergo an A-B conformational transition (see Fig. 14) (62). This phase transformation is thus first order, and besides being a conformational transition for single DNAs, is connected also with the melting of the base stacking as well as positional order of the helices in the lattice. The ensuing low-density mesophase, where DNA is in the B conformation, is therefore characterized by short range base stacking order, short range 2-dimensional positional order and long-range bond orientational order (Fig. 15) (63). This order is connected with the spatial direction of the nearest neighbors (64). It is for this reason that the phase has been termed a "line hexatic" phase. Hexatics usually occur only in 2-dimensional systems. They have crystalline bond orientational order but liquidlike positional order. There might be a hexatic-hexagonal columnar transition somewhere along the hexatic line, though a direct experimental proof is lacking.

The difference between the 2 phases is that the hexagonal columnar phase has also a crystalline positional order and is thus a real 2-dimensional crystal (see Fig. 15) (65). It is the long-range bond orientational order that gives the line hexatic phase some crystalline character (66). The DNA duplexes are still packed in parallel, while the local symmetry perpendicular to the long axes of the molecules is changed to hexagonal. The directions of the nearest neighbors persist through macroscopic dimensions (on the order of mm) while their positions tend to become disordered already after several (typically 5 to 10) lattice spacings. This mesophase has a characteristic X-ray scattering fingerprint (see Fig. 15). If the X-ray beam is directed parallel to the long axis of the molecules, it will show a hexagonally symmetric diffraction pattern of broad liquidlike peaks (67).

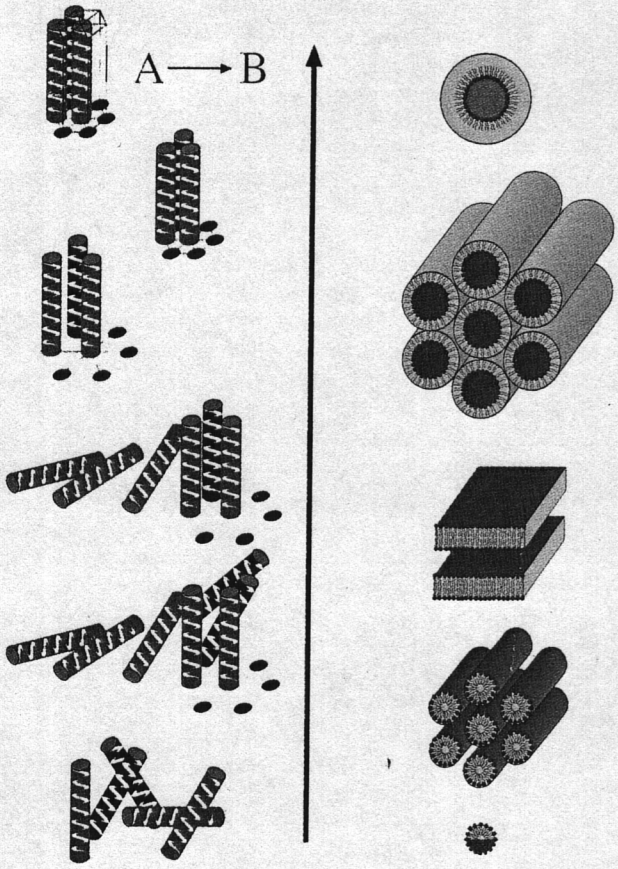

Figure 14 Schematic phase diagrams for DNA (left) and lipids (right). In both cases, the arrow indicates increasing density in both cases. DNA starts (bottom) as a completely disordered solution. It progresses through a sequence of blue phases characterized by cholesteric pitch in two perpendicular directions (68), then to a cholesteric phase with pitch in only one direction. At still larger densities, this second cholesteric phase is succeeded by a hexatic phase, characterized by short-range, liquidlike positional order and long-range, crystallike bond orientational (or hexatic order, indicated by lines). At highest densities, there is a crystalline phase characterized by long-range positional order of the molecules and long-range base stacking order in the direction of the long axes of the molecules. Between the hexatic and the crystalline forms, there might exist a hexagonal columnar liquid-crystalline phase, that is similar to a crystal, but with base stacking order only on short scales. The lipid-phase diagram (77) is a composite of results obtained for different lipids. It starts from a micellar solution and progresses through a phase of lipid tubes to a multilamellar phase of lipid bilayers. This is followed by an inverted hexagonal columnar phase of water cylinders and possibly goes to an inverted micellar phase. Most lipids show only a subset of these possibilities. Boundaries between the phases shown here might contain exotic cubic phases not included in this picture. See the color insert for a color version of this figure.

Typical lattice spacings in the line hexatic phase are between 25 and 35 Å (i.e., between 600 and 300 mg/mL of DNA) (63). The free energy in this mesophase is mostly a consequence of the large hydration forces stemming from removal of water from the phosphates of the DNA backbone. Typically independent of the ionic strength of the bathing solution, these hydration forces (54) depend exponentially on the interhelical separation and decay with a decay length of about 3 Å (11) at these large densities. This value of the hydration decay length seems to indicate that it is determined solely by the bulk properties of the solvent (i.e., water).

It is interesting to note that the behavior of short-fragment DNA in this range of concentrations is different from the long DNA (65). The short-fragment DNA, typically the nucleosomal DNA fragment of 146 bp, makes a 2-dimesional hexagonal phase at interaxial spacing of ~30 Å, that progressively orders into a 3-dimensional hexagonal phase on decrease of the interaxial spacing to ~23 Å (65). At still larger concentrations, the short-fragment DNA makes a 3-dimensional orthorhombic crystal, with a deformed hexagonal unit cell perpendicular to the *c*-axis. Concurrently to this symmetry transformation, the helical pitch of the condensed phase decreases continuously from 34.6 to 30.2 Å (65). The reasons for this fundamental difference between the behavior of long as opposed to short-fragment DNA is still not well understood.

When the osmotic pressure is lowered to about 10 atm (corresponding to interaxial spacing of about 35 Å, or DNA density of about 300 mg/mL), the characteristic hexagonal X-ray diffraction fingerprint of the line hexatic mesophase disappears continuously. This disappearance suggests the presence of a continuous, second-order transition into a low-density cholesteric (63). It is characterized by short-range (or effectively no) base stacking order, short-range positional order, short-range bond orientational order, but long-range cholesteric order, manifested in a continuing rotation of the long axis of the molecules in a preferred direction. In this sense, the cholesteric DNA mesophase would retain the symmetry of a 1-dimensional crystal. X-ray diffraction pattern of the DNA in the cholesteric phase is isotropic and has the form of a ring. Crossed polarizers, however, reveal the existence of long-range cholesteric order just as in the case of short chiral molecules. The texture of small drops of DNA cholesteric phase (spherulites) under crossed polarizers (Fig. 16) reveals the intricacies of orientational packing of DNA, where its local orientation is set by a compromise between interaction forces and macroscopic geometry of a spherulite. It is thus only at these low densities that the chiral character of the DNA finally makes an impact on the symmetry of the mesophase. It is not yet fully understood why the chiral order is effectively screened from the high-density DNA mesophases.

At still smaller DNA densities, the predominance of the chiral interactions in the behavior of the system remains. Recent work on the behavior of low-density DNA mesophases indicates (68) that the cholesteric part of the phase diagram might end with a sequence of blue phases that would emerge as a consequence of the loosened packing constraints coupled to the chiral character of the DNA molecule. At DNA density

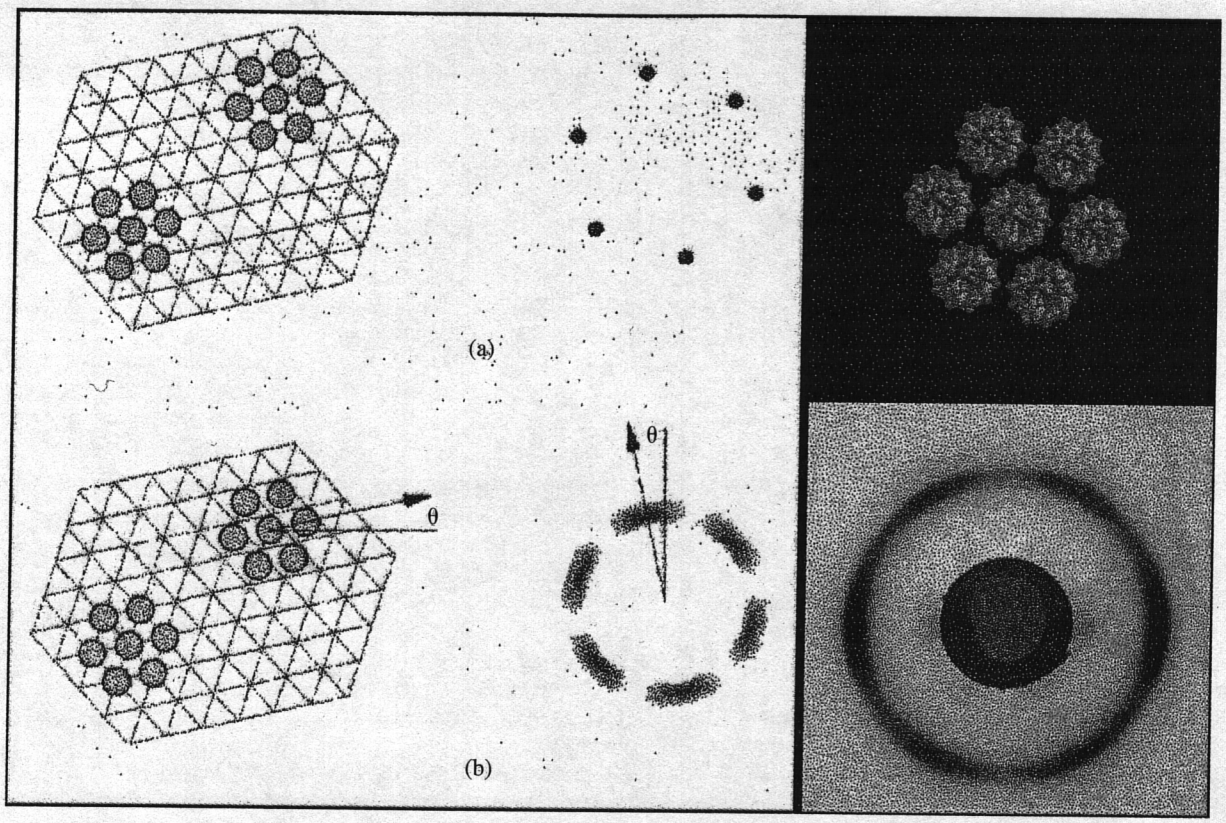

Figure 15 Bond orientational or hexatic order. With a real crystal if one translates part of the crystal by a lattice vector, the new position of the atoms completely coincides with those already there. (Adapted from ref. 67.) In a hexatic phase the directions to the nearest neighbors (bond orientations) coincide (after rotation by 60°), but the positions of the atoms do not coincide after displacement in 1 of the 6 directions! Consequently, a real crystal gives a series of very sharp Bragg peaks in X-ray scattering (upper half of box), whereas a hexatic gives hexagonally positioned broad spots. The pattern of X-ray scattering by high- density DNA samples gives a fingerprint of a hexatic phase. The densitogram of the scattering intensity (right half of figure) shows 6 pronounced peaks that can be Fourier decomposed with a marked sixth-order Fourier coefficient, another sign that that the scattering is due to long-range bond orientational order (63). See the color insert for a color version of this figure.

of about 10 mg/mL, the cholesteric phase line would end with DNA reentering the isotropic liquid solution where it remains at all subsequent densities, except perhaps at very small ionic strengths (69).

G. DNA Equation of State

The free energy of the DNA cholesteric mesophase appears to be dominated by the large elastic shape fluctuations of its constituent DNA molecules (70) that leave their imprint in the very broad X-ray diffraction peak (55). Instead of showing the expected exponential decay characteristic of screened electrostatic interactions (71), where the decay length is equal to the Debye length, it shows a fluctuation-enhanced repulsion similar to the Helfrich force existing in the flexible smectic multilamellar arrays (41). Fluctuations not only boost the magnitude of the existing screened electrostatic repulsion, but also extend its range through a modified decay length equal to 4 times the Debye length. The factor-of-4 enhancement in the range of the repulsive force is a consequence of the coupling between the bare electrostatic repulsions of exponential type and the thermally driven elastic shape fluctuations described through elastic curvature energy that is proportional to the square of the second derivative of the local helix position (42). In the last instance, it is a consequence of the fact that DNAs in the array interact via an extended, soft-screened electrostatic potential and not through hard bumps as assumed in the simple derivation in Chapter 2.

The similarity of the free energy behavior of the smectic arrays with repulsive interactions of Helfrich type and the DNA arrays in the cholesteric phase that can also be understood in the framework of the Helfrich-type-enhanced repulsion satisfies a consistency test for our understanding of flexible supermolecular arrays.

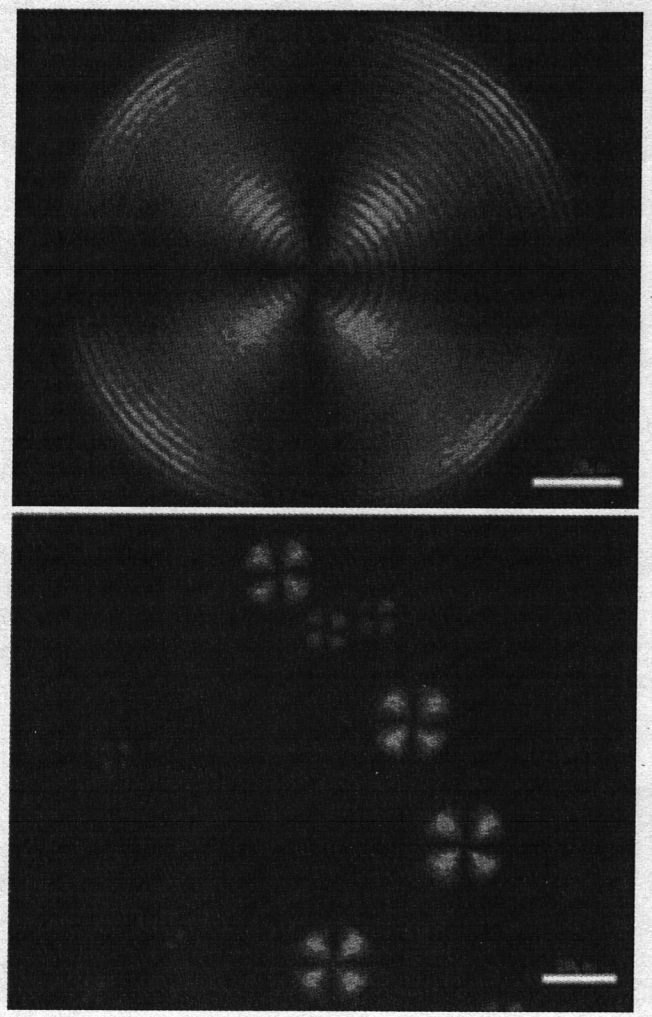

Figure 16 Texture of small drops of DNA cholesteric phase (spherulites) in a PEG solution under crossed polarizers. These patterns reveal the intricacies of DNA orientational packing when its local orientation is set by a compromise between interaction forces and the macroscopic geometry of a spherulite. The change from a bright to a dark stripe indicates that the orientation of the DNA molecule has changed by 90 degrees.

IV. LIPID MESOPHASES

A. Aggregation of Lipids in Aqueous Solutions

Single-molecule solutions of biological lipids exist only over a negligible range of concentrations; virtually all interesting lipid properties are those of aggregate mesophases such as bilayers and micelles. Lipid molecules cluster into ordered structures to maximize hydrophilic and minimize hydrophobic interactions (72,73). These interactions include negative free energy contribution from the solvation of polar heads and van der Waals interactions of hydrocarbon chains, competing with positive contributions such as steric, hydration, and electrostatic repulsions between polar heads. The "hydrophobic effect," which causes segregation of polar and nonpolar groups, is said to be driven by the increase of the entropy of the surrounding medium.

Intrinsic to the identity of surfactant lipids is the tension between water-soluble polar groups and lipid-soluble hydrocarbon chains. There is no surprise then that the amount of water available to an amphiphile is a parameter pertinent to its modes of packing and to its ability to incorporate foreign bodies.

These interactions therefore force lipid molecules to self-assemble into different ordered microscopic structures, such as bilayers, micelles (spherical, ellipsoidal, rodlike, or disk-like), which can, especially at higher concentrations, pack into macroscopically ordered phases, such as lamellar, hexagonal, inverted hexagonal, and cubic. The morphology of these macroscopic phases changes with the balance between attractive van der Waals and ion correlation forces vs. electrostatic, steric, hydration, and undulation repulsion (74).

B. The Lipid Bilayer

The workhorse of all lipid aggregates is the bilayer (Fig. 17) (73). This sandwich of two monolayers, with nonpolar hydrocarbon chains tucked in toward each other and polar groups facing water solution, is only about 20 to 30 Å thick. Yet it has the physical resilience and the electrical resistance to form the plasma membrane that divides "in" from "out" in all biological cells. Its mechanical properties have been measured in terms of bending and stretching moduli. These strengths together with measured interactions between bilayers in multilamellar stacks have taught us to think quantitatively about the ways in which bilayers are formed and maintain their remarkable stability.

With some lipids, such as double-chain phospholipids, when there is the need to encompass hydrocarbon components voluminous compared with the size of polar groups, the small surface-to-volume ratio of spheres, ellipsoids, or even cylinders cannot suffice even at extreme dilution. Bilayers in this case are the aggregate form of choice. These may occur as single "unilamellar" vesicles, as onionlike multilayer vesicles, or multilamellar phases of indefinite extent. In vivo, bilayer-forming phospholipids create the flexible but tightly sealed plasma-membrane matrix that defines the inside from the outside of a cell. In vitro, multilayers are often chosen as a matrix of choice for the incorporation of polymers. Specifically, there are tight associations between positively charged lipids that merge with negatively charged DNA in a variety of forms (see below).

The organization of lipid molecules in the bilayer itself can vary (73). At low enough temperatures or dry enough conditions the lipid tails are frozen in an all-trans conformation that minimizes the energy of molecular bonds in the alkyl tails of the lipids. Also, the positions of the lipid heads along the surface of the bilayer are frozen in 2-dimensional positional order, making the overall conformation of the lipids in

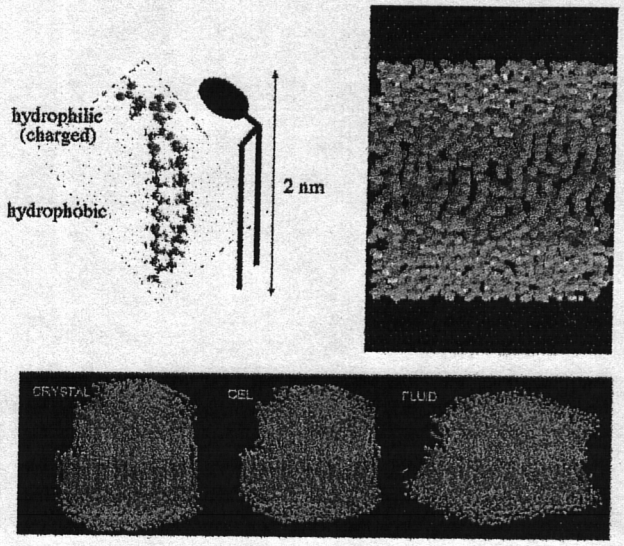

Lipid	Bending rigidity [10^{-19}J]	Area compression [mN/m]
DMPC	1.15	145
SOPC	0.9	200
EggPC	0.4-2	
Plasma membrane	0.2-2	700
Red Blood Cell	0.13 - 0.3	450

Figure 17 The lipid bilayer. A lipid molecule has a hydrophilic and a hydrophobic part (here shown is the phosphatidylserine molecule that has a charged headgroup). At high-enough densities, lipid molecules assemble into a lipid bilayer. Together with membrane proteins as its most important component the lipid bilayer is the underlying structural component of biological membranes. The degree of order of the lipids in a bilayer depends drastically on temperature and goes through a sequence of phases (see main text): crystalline, gel, and fluid, depicted in the middle drawing. The box at bottom gives sample values of bilayer bending rigidity and area compressibility for some biologically relevant lipids and one well-studied cell membrane. See the color insert for a color version of this figure.

the bilayer crystal (L_C). The chains can either be oriented perpendicular to the bilayer surface (L_β and $L_{\beta'}$) or be tilted (crystalline phase L_C or ripple phase P_β). Such a crystalline bilayer cannot exist by itself but assembles with others to make a real 3-dimensional crystal.

Upon heating, various rearrangements in the 2-dimensional crystalline bilayers occur, first the positional order of the headgroups melts leading to a loss of 2-dimensional order ($L_{\beta'}$) and tilt (L_β), then, at the gel–liquid crystal phase transition the untilted or rippled (P_β phase) bilayer changes into a bilayer membrane with disordered polar heads in 2 dimensions and conformationaly frozen hydrocarbon chains, allowing them to spin around the long axes of the molecules, the so-called L_α phase. At still higher temperatures, the thermal disorder finally also destroys the ordered configuration of the alkyl chains, leading to a fluidlike bilayer phase. The fluid bilayer phase creates the fundamental matrix that according to the fluid mosaic model (72) contains different other ingredients of biological membranes (e.g., membrane proteins, channels, etc.).

Not only bilayers in multilamellar arrays but also liposome bilayers can undergo such phase transitions; electron microscopy has revealed fluid phase, rippled, and crystalline phase in which spherical liposomes transform into polyhedra due to very high values of bending elasticity of crystallized bilayers (75).

The fluid phase of the lipid bilayer is highly flexible. This flexibility makes it prone to pronounced thermal fluctuations, resulting in large excursions away from a planar shape. This flexibility of the bilayer is essential for understanding the zoo of equilibrium shapes that can arise in closed bilayer (vesicles) systems (76). Also, just as in the case of flexible DNA, it eventually leads to configurational entropic interactions between bilayers that have been crammed together (41). Bilayers and linear polyelectrolytes thus share a substantial amount of fundamentally similar physics that allows us to analyze their behavior in the same framework.

C. Lipid Polymorphism

Low temperature phases (77) are normally lamellar with frozen hydrocarbon chains tilted (crystalline phase L_C or ripple phase P_β) or nontilted (L_β and $L_{\beta'}$ form three-, two-, or one-D crystalline or gel phases) with respect to the plane of the lipid bilayers. Terminology from thermotropic liquid crystals phenomenology (50) can be used efficiently in this context: these phases are smectic, and SmA describes 2-dimensional fluid with no tilt while a variety of SmC phases with various indices encompass tilted phases with various degrees of 2-dimensional order. Upon melting, liquid crystalline phases with 1- (lamellar L_α), 2- (hexagonal II), or 3-dimensional (cubic) positional order can form.

The most frequently formed phases are micellar, lamellar, and hexagonal (Fig. 14). Normal hexagonal phase consists of long cylindrical micelles ordered in a hexagonal array, while in the inverse hexagonal II (H_{II}) phase water channels of inverse micelles are packed hexagonally with lipid tails filling the interstices. In excess water, such arrays are coated by a lipid monolayer. The morphology of these phases can be maintained upon their (mechanical) dispersal into colloidal dispersions. Despite that energy has to be used to generate dispersed mesophases relatively stable colloidal dispersions of particles with lamellar, hexagonal, or cubic symmetry can be formed.

Many phospholipids found in lamellar cell membranes, after extraction, purification, and resuspension, prefer an inverted hexagonal geometry (Fig. 18) (77). Under excess-water conditions different lipids will assume different most-favored spontaneous radii for the water cylinder of this inverted phase (78). An immediate implication is that different lipids are strained to different degrees when forced into lamellar pack-

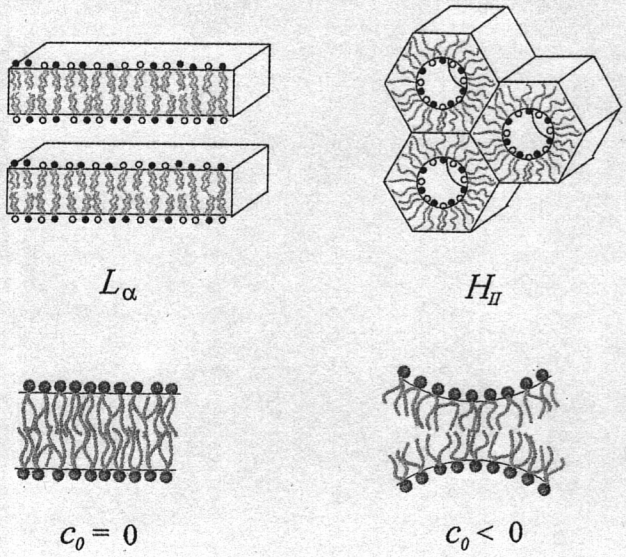

Figure 18 Different lipids are strained to different degrees when forced into lamellar packing. Relaxation of this strain contributes to the conditions for lamellar–to–inverted hexagonal phase transitions that depend on temperature, hydration, and salt concentration (for charged lipids). See the color insert for a color version of this figure.

ing. There are lamellar-inverted hexagonal phase transitions that occur with varied temperature, hydration, and salt concentration (for charged lipids) that form in order to alleviate this strain (see Fig. 18).

In the presence of an immiscible organic phase emulsion, droplets can assemble (79). In regions of phase diagram that are rich in water, oil-in-water emulsions and microemulsions ($c > 0$) can be formed, while in oil-rich regions these spherical particles have negative curvature and are therefore water-in-oil emulsions. The intermediate phase between the two is a bicontinuous emulsion that has zero average curvature and an anomalously low value of the surface tension (usually brought about the use of different cosurfactants) between the two immiscible components. Only microemulsions can form spontaneously (analogously to micelle formation) while for the formation of a homogeneous emulsion some energy has to be dissipated into the system.

The detailed structure of these phases as well as the size and shape of colloidal particles are probably dominated by:

- The average molecular geometry of lipid molecules
- Their aqueous solubility and effective charge
- Weaker interactions such as intra- and intermolecular hydrogen bonds
- Stereoisomerism as well as interactions within the medium

All depend on the temperature, lipid concentration, and electrostatic and van der Waals interactions with the solvent and solutes. With charged lipids, counterions, especially anions, may also be important. Ionotropic transitions have been observed with negatively charged phospholipids in the presence of metal ions leading to aggregation and fusion (80). In cationic amphiphiles, it was shown that simple exchange of counterions can induce micelle-vesicle transition. Lipid polymorphism is very rich and even single-component lipid systems can form a variety of other phases, including ribbonlike phases, coexisting regions and various stacks of micelles of different shapes.

D. Forces in Multilamellar Bilayer Arrays

Except for differences in dimensionality, forces between bilayers are remarkably similar to those between DNA. At very great separations between lamellae, the sheetlike structures flex and "crumple" because of (thermal) Brownian motion (41). Just as an isolated flexible linear polymer can escape from its 1 linear dimension into the 3 dimensions of the volume in which it is bathed, so can 2-dimensional flexible sheets. In the most dilute solution, biological phospholipids will typically form huge floppy closed vesicles; these vesicles enjoy flexibility while satisfying the need to keep all greasy nonpolar chains comfortably covered by polar groups rather than exposed at open edges. For this reason, in very dilute solution, the interactions between phospholipid bilayers are usually space wars of collision and volume occupation. This steric competition is always seen for neutral lipids; it is not always true for charged lipids (74).

Especially in the absence of any added salt, planar surfaces emit far-ranging electrostatic fields (27) that couple to thermally excited elastic excursions to create very long-range repulsion (44,83). As with DNA, this repulsion is a mixture of direct electrostatic forces and soft collisions mediated by electrostatic forces rather than by actual bilayer contact. In some cases electrostatic repulsion is strong enough to snuff out bilayer bending when bilayers form ordered arrays with periodicities as high as hundreds of Å (82).

Almost always bilayers align into well-formed stacks when their concentration approaches ~50 to 60 weight percent and their separation is brought down to a few tens of Å. In this region charged layers are quite orderly with little lamellar undulation. In fact, bilayers of many neutral phospholipids often spontaneously fall out of dilute suspension to form arrays with bilayer separations between 20 and 30 Å. These spontaneous spacings are believed to reflect a balance between van der Waals attraction and undulation-enhanced hydration repulsion (74). One way to test for the presence of van der Waals forces has been to add solutes such as ethylene glycol, glucose, or sucrose to the bathing solutions. It is possible then to correlate the changes in spacing with changes in van der Waals forces due to the changes in dielectric susceptibility as described above (83). More convincing, there have been direct measurements of the work to pull apart bilayers that sit at spontaneously assumed spacings. This work of separation is of the magnitude expected for van der Waals attraction. (84).

Similar to DNA, multilayers of charged or neutral lipids subjected to strong osmotic stress reveal exponential variation in osmotic pressure vs. bilayer separation (74). Typically at separations between dry "contact" and 20 Å, exponential decay lengths are 2 to 3 Å in distilled water or in salt solution, whether phospholipids are charged or neutral. Lipid bilayer repulsion in this range is believed to be due to the work of polar group dehydration sometimes enhanced by lamellar collisions from thermal agitation (85). Normalized per area of interacting surface the strength of hydration force acting in lamellar lipid arrays and DNA arrays is directly comparable.

Given excess water, neutral lipids will usually find the above-mentioned separation of 20 to 30 Å at which this hydration repulsion is balanced by van der Waals attraction. Charged lipids, unless placed in solutions of high salt concentration, will swell to take up indefinitely high amounts of water. Stiff charged bilayers will repel with exponentially varying electrostatic double layer interactions, but most charged bilayers will undulate at separations where direct electrostatic repulsion has weakened. In that case, similar to what has been described for DNA, electrostatic repulsion is enhanced by thermal undulations (86).

E. Equation of State of Lipid Mesophases

Lipid polymorphism shows much less universality that DNA. This is of course expected because lipid molecules come in many different varieties (73) with strong idiosyncrasies in terms of the detailed nature of their phase diagrams. One thus can not achieve the same degree of generality and universality in the description of lipid phase diagram and consequent equations of state as was the case for DNA.

Nevertheless, recent extremely careful and detailed work on PCs by J. Nagle and his group (87) points strongly to the conclusion that at least in the lamellar part of the phase diagram of neutral lipids the main features of the DNA and lipid membrane assembly physics indeed is the same (85). This statement however demands qualification. The physics is the same, provided one first disregards the dimensionality of the aggregates—1 dimensional in the case of DNA and 2 dimensional in the case of lipid membranes—and takes into account the fact that while van der Waals forces in DNA arrays are negligible, they are essential in lipid membrane force equilibria. One of the reasons for this state of affairs is the large difference, unlike in the case of DNA, between the static dielectric constant of hydrophobic bilayer interior, composed of alkyl lipid tails, and the aqueous solution bathing the aggregate.

We have already pointed out that in the case of DNA arrays quantitative agreement between theory, based on hydration and electrostatic forces augmented by thermal undulation forces, and experiment has been obtained and extensively tested (7,42). The work on neutral lipids (85) claims that the same level of quantitative accuracy can be achieved also in lipid membrane assemblies if one takes into account hydration and van der Waals forces again augmented by thermal undulations. Of course, the nature of the fluctuations in the 2 systems is different and is set by the dimensionality of the fluctuating aggregates—1- vs. 2-dimensional.

The case of lipids adds an additional twist to the quantitative link between theory and experiments. DNA in the line hexatic as well as cholesteric phases (where reliable data for the equation of state exist) is essentially fluid as far as positional order is concerned and thus has unbounded positional fluctuations. Lipid membranes in the smectic multilamellar phase are quite different in this respect. They are not really fluid as far as positional order is concerned but show something called quasilong range (QLR) order, meaning that they are in certain respects somewhere between a crystal and a fluid (50,67). The quasi long-range positional order makes itself recognizable through the shape of the X-ray diffraction peaks in the form of persistent (Caille) tails (67).

In a crystal one would ideally expect infinitely sharp peaks with Gaussian broadening only because of finite accuracy of the experimental setup. Lipid multilamellar phases, however, show peaks with very broad, non-Gaussian, and extended tails that are one of the consequences of QLR positional order. The thickness of these peaks for different orders of X-ray reflexions varies in a characteristic way with the order of the reflexion (67). It is this property that allows us to measure not only the average spacing between the molecules, but also the amount of fluctuation around this average spacing. Luckily, the theory also predicts that and without any free parameters (all of them being already determined from the equation of state) the comparison between predicted and measured magnitude in positional fluctuations of membranes in a multilamellar assembly is more than satisfactory (85).

In summing up, the level of understanding of the equation of state reached for DNA and neutral lipid membrane arrays is pleasing.

V. DNA–LIPID INTERACTIONS

Mixed in solution with cationic lipids (CLs), DNA spontaneously forms CL-DNA aggregates of submicron size. These DNA-lipid aggregates, sometimes called "lipoplexes," (88) are routinely used for cell transfection in vitro. More important, they are used primarily as potential gene delivery vehicles for in vivo gene therapy [for recent reviews, see (89–94) and references therein]. Under appropriate conditions these aggregates reveal complex underlying thermodynamic phase behavior. There is a practical paradox here. We use stable equilibrium structures to reveal the forces that cause aggregation and assembly; we use this knowledge of forces to create the unstable preparations likely to be most efficient in transfection.

Lipoplexes for transfection were first proposed by Felgner and coworkers (95,96). The guiding idea was to overcome the electrostatic repulsion between cell membranes (containing negatively charged lipids) and negative DNA by complexing DNA with positively charged CL. Preliminary experimental data showed that at least some lipoplexes deliver DNA through direct fusion with the cell membrane (97). More often,

however, lipoplex internalization probably proceeds through endocytosis after initial interaction with the cell's membrane.

Prior to the attempts to use lipoplexes for transfection, studies of DNA aggregated with multivalent cations and coated with negatively charged liposomes were also explored as possible vectors. It was hoped that CL-DNA complexes would no longer require an additional complexing agent, and that also, the transfection efficiency would be higher. The complex's lipid coating could protect the tightly packed DNA cargo during its passage to the target cells.

Although not confronted with the immunological response, risked by the alternative viral vector strategy, the use of lipoplexes in gene therapy is still hampered by toxicity of the CL and low in vivo tranfection efficiency, despite the in vitro efficiency of some CL formulations. This discrepancy can be attributed to the multistage and multibarrier process the complexes must endure before transfection is achieved. These steps typically include passage in the serum, interaction with target and other cells, internalization, complex disintegration in the cytoplasm, transport of DNA into the nucleus, and ultimately expression.

In the search for increasingly more potent gene delivery vectors, the intimate relationship between the lipoplex's phase structure (or morphology) and its transfection efficiency probably serves as the greatest motivation for their study. How is transfection affected by lipoplex morphology? How may this structure be controlled? Experiment and theory of the past decade shed some light on such fundamental questions. They may give perspective for future strategies to design CL-based nonviral vectors.

To this end, we present our current understanding of the structure and phase behavior of CL-DNA complexes. We review the relation of structure to transfection efficiency and, more specifically, to the way the complex formation overcomes one barrier to DNA release into the cytoplasm.

A. Structure of CL-DNA Complexes

In general, the structures of CL-DNA composite phases can be viewed as morphological hybrids of familiar pure-lipid and pure-DNA phases. A first example is the lamellarlike structure initially proposed by Lasic at al. (99,100). The first comprehensive and unambiguous evidence for this structure came from a series of studies by Rädler et al. (101–105). From high-resolution synchrotron X-ray diffraction and optical microscopy, they reported the existence of novel lamellar CL-DNA phase morphologies. In particular, one complex structure was shown to consist of lamellar multilayer. In this case smecticlike stacks of mixed bilayers, each composed of a mixture of CL—for example, dioleoyltrimethylammonium propane (DOTAP)—and neutral "helper" lipid—for example, dioleoylphosphatidylcholin (DOPC)—with monolayers of DNA strands intercalated within the intervening water gaps (Fig. 19A), like a multilipid bilayer L_α phase (106). Helper lipids are often added for their fusogenic properties. Dioleoylphosphatidylethanol amine (DOPE), for example, is conjectured to promote transfection. In addition, because pure (synthetically derived) cationic lipids often tend to form micelles in solution, helper lipids facilitate the formation of membranes.

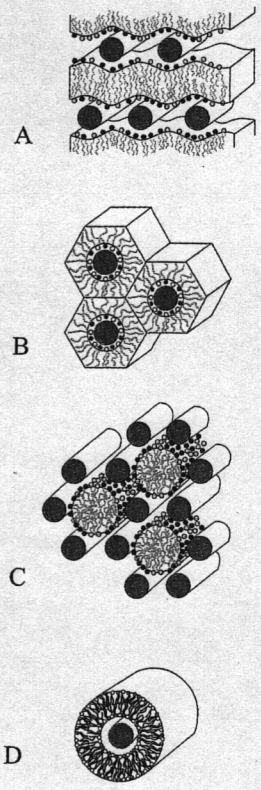

Figure 19 Schematic illustration of some possible structures of DNA–mixed lipid (cationic/nonionic) complexes. (A) The sandwichlike (L^c_α) lamellar complex composed of parallel DNA molecules intercalated between lipid bilayers. (B) The honeycomblike (H^c_{II}) hexagonal complex, composed of a hexagonally packed bundle of monolayer-coated DNA strands. (C) Two interpenetrating hexagonal lattices, one of DNA, the other of micelles. (D) Spaghetti-like complex, composed of bilayer-coated DNA. (Reprinted by permission from Ref. 143, Biophysical Society.) See the color insert for a color version of this figure.

In this L^c_α complex geometry, the DNA strands within each gallery are parallel to each other, exhibiting a well-defined repeat distance d. While d depends on the CL/DNA and CL/HL concentration ratios, the spacing between two apposed lipid monolayers is nearly constant at ~26 Å, corresponding to the diameter of double-stranded B-DNA, ca. 20 Å, surrounded by a thin hydration shell. This L^c_α lamellar ("sandwich") complex is stabilized by the electrostatic attraction between the negatively charged DNA and the cationic lipid bilayer. Because of strong electrostatic repulsion between the charged bilayers (particularly at low salt conditions), the lamellar lipid phase is unstable without DNA.

Quite different equilibrium ordered phase morphologies were found to occur from other choices of neutral helper lipid (HL). In the case of DOPE, or lecithin, for example, inverted hexagonal (''honeycomb'' or H_{II}^{c}) organization of the lipid, with stretches of double-stranded DNA lying in the aqueous solution regions, were found to form, see Fig. 19B (95,102,107). The H_{II}^{c} structure may be regarded as the inverse-hexagonal (H_{II}) lipid phase, with DNA strands wrapped within its water tubes. Here, too, the diameter of the water tubes is only slightly larger than the diameter of the DNA ''rods.'' The presence of DNA is crucial for stabilizing the hexagonal structure. Without it, strong electrostatic repulsion will generally drive the lipids to organize themselves into planar bilayers. In fact, the most abundant aggregate structure of pure CL and HL mixtures, from which hexagonal complexes are subsequently formed, is single-bilayer liposomes.

Other CL-DNA phases have also been observed. One of the earliest studies probing the structure of lipoplexes showed some evidence for an hexagonal arrangement of rodlike micelles intercalated between hexagonally packed DNA, Fig. 19C (108,109). The number of possibilities is even larger if one also considers metastable intermediates. The ''spaghetti'' structure (see Fig. 19D), observed using freeze-fracture electron microscopy, has been predicted by theory to probably be one such metastable morphology (110,111). Here, each (possibly supercoiled) DNA strand is coated by a cylindrical bilayer of the CL/HL lipid mixture (112,113). Early proposed models of the CL-DNA complexes suggested a ''beads on a string'' type complex, in which the DNA is wrapped around or in between lipid vesicles (and even spherical micelles). Although this may not turn out to be an equilibrium structure, such aggregates are sometimes found, and may also serve as unstable intermediates (114–116). Other structures, such as the bilamellar invaginated liposomes (BIV) made of DOTAP-Chol, have been proposed and demonstrated to be efficient vectors (97,117). These structures resemble to some degree the L_{α}^{c} phase. However, formed from extruded liposomes, the BIVs are most probably metastable.

What factors determine which of these phases (or possibly several coexisting structures) actually form in solution? To what degree can we control and predict them? Control can first be achieved through the choice of type of CL and HL, and the ratio between the 2 used in forming liposomes. This in turn will determine such basic properties as the lipid bilayer's bending rigidity, spontaneous curvature, and surface charge density of the water–lipid aggregate interface. An additional experimentally controllable parameter is the ratio between the lipid and DNA content in solution. Both these parameters, we show, have significant effects on the phases that are formed.

B. Counterion Release

From the start, it was realized that the expected condensation of DNA with oppositely charged lipids could be used to package and send DNA to transfect targeted cells. The expectation that the DNA and lipids would aggregate was intuitively based on the notion that oppositely charged bodies attract. Early experiments confirmed the aggregation of DNA and lipids. However, the mechanism by which CL and DNA were found to associate—previously termed in the context of macromolecular association ''counterion release'' (118)—is more intricate than the ''opposites attract'' mechanism that may be naively expected.

Prior to association, DNA and lipids are bathed in the aqueous solutions containing their respective counterions, so that the solutions are overall electrostatically neutral. The counterions are attracted to the oppositely charged macromolecules, thus gaining electrostatic energy. Here, in addition to DNA, we also refer to the preformed CL liposomes as a ''macromolecules'' because they typically retain their integrity in solution, even upon association with other charged macromolecules. The counterions are therefore confined to the vicinity of the oppositely charged macromolecules at the compromise of greater translational entropy in solution.

Upon association, the 2 oppositely charged macromolecules condense to form CL-DNA complexes (Fig. 20). Many (possibly all) previously confined counterions can now be expelled into the bulk solution from the lipoplex interior, thus gaining translational entropy. Although the translational entropy of the paired macromolecules is reduced by (typically) only a few k_BTs (due to loss of conformational and translational entropy), many released counterions can now favorably contribute to a gain in entropy, each by a comparable amount. For this reason it is sometimes stated that the DNA–lipid condensation is ''entropically driven.'' The electrostatic en-

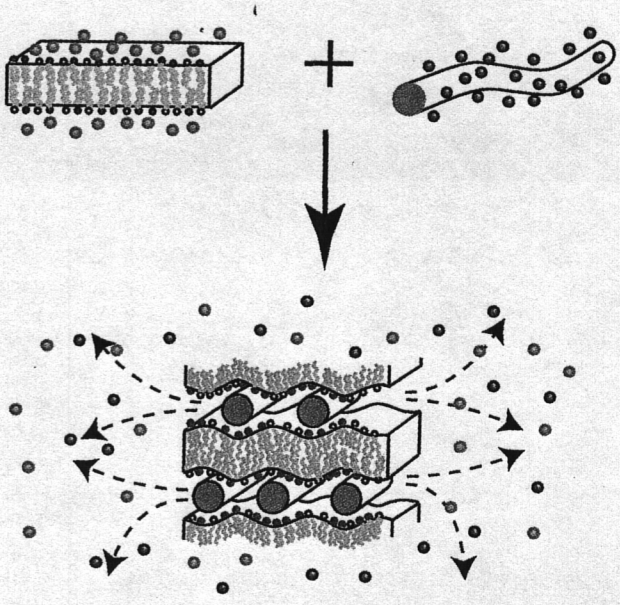

Figure 20 Schematic illustration of the condensation of DNA and lipid bilayers (liposomes) into CL-DNA complexes. In the process, the previously confined counterions are released into the bathing solution, thereby gaining translational entropy. See the color insert for a color version of this figure.

ergy can also contribute somewhat to stabilizing the lipoplexes. However, it has been well argued, both experimentally and theoretically, that the cardinal contribution to the association free energy of CL–DNA complexes is the entropy gain associated with counterion release (119,120).

Further support was given by counting released ions, using conductivity measurements of the supernatant. It was possible to determine that a maximal number of counterions were released when the number of "fixed" charges on the DNA and lipid were exactly equal.

Calorimetric measurements confirm this finding and find furthermore that the association could in fact be endothermic, so that it is only favorable for entropic reasons (121,122). The special point at which the number of positive and negative fixed charges is equal has been termed the "isoelectric point." At this point, the (charging) free energy of the complex is minimal: the fixed charges of opposite signs fully compensate each other, thus allowing essentially all the counterions to be released into solution. Note, that by "counterions" we do not refer here to added salt ions. Ions of added salt will span the entire solution, including the lipoplex interior. Thus, the salt content changes the thermodynamic phase behavior and the value of the adsorption free energy, mainly because a high ambient salt concentration lowers the entropic gain associated with releasing a counterion.

Theoretical predictions and estimates from calorimetry show that for a salt solution of concentration $n^0 = 4$ mM, and a 1:1 CL/HL mole ratio, the gain in free energy upon adsorption at the isoelectric point is a bemusingly large ~7.5 k_BT per fixed charge pair (DNA and CL) (120–122). This value translates to over 2000 k_BT when considering the energy per persistence length of DNA (about 50 nm), carrying approximately 300 charges.

C. Lamellar DNA–lipid Complexes

Many degrees of freedom with competing contributions are expected to ultimately determine the free energy minimum for equilibrium DNA/membrane structures. Typically, these include (but are not limited to) electrostatic energy, elastic bending, solvation, van der Waals, ion mixing, and lipid mixing. Therefore, considering the lipoplex phase behavior, we begin for simplicity by discussing systems where only L_α^c complexes are found. This can be expected when the lipid membranes are rather rigid, such as in the case of mixtures of DOTAP/DOPC (89,102) or DMPC/DC-Chol (123). The main structural parameter for the L_α^c phase is the DNA–DNA distance, reflecting the DNA packing density within the complex. A series of X-ray measurements by Rädler et al. revealed how the DNA–DNA spacings d vary with the ratio ρ of the number of lipid charges to the total number of charges on DNA. The measurements were repeated for each of several different lipid compositions defined by the ratio of charged to overall number of lipids, ϕ. It was found that for a lipid mixture of a given composition ϕ, the spacings are constant throughout the low ρ range where the complex coexists with excess DNA. In the high ρ range, where the complex coexists with excess lipid, the spacings are also nearly constant. Inbetween these limits there exists a "single-phase" region, where all the DNA and lipids participate in forming lipoplexes. This region is generally found to include the isoelectric point where, by definition, $\rho = 1$ (Fig. 21).

Several theoretical studies have been proposed to account for this phase behavior (119,124,125). It was found that it is possible to account for most of the experimental observations within the scope of the nonlinear Poisson–Boltzmann equation (125). In this theoretical model, elastic deformations of

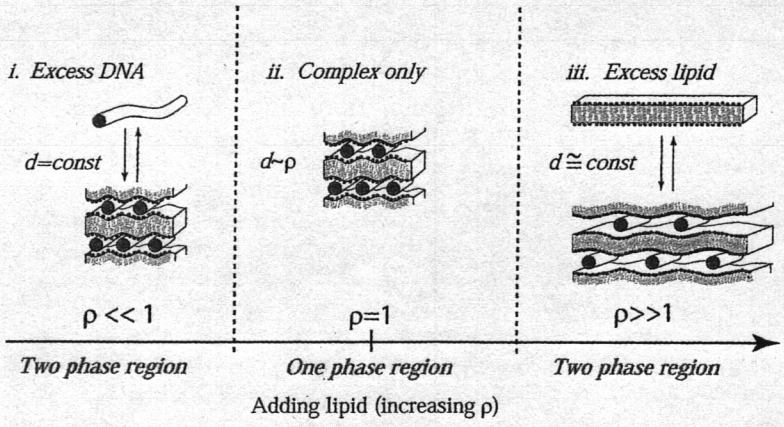

Figure 21 Schematic illustration of the phase evolution of the L_α^c complexes for a constant lipid composition (cationic to nonionic lipid ratio). As lipid is added (ρ increases), the systems evolve from a 2-phase (complex and excess DNA) region through a 1-phase (complex only) region, and finally to a 2-phase (complex and excess lipid) region. The isoelectric point is generally contained within the 1-phase region. See the color insert for a color version of this figure.

the DNA and lipid bilayers were neglected, treating them as rigid macromolecules. On the other hand the lipid's lateral (in plane) mobility in the membrane layer was explicitly taken into account. This turns out to be an important degree of freedom in mixed fluid bilayers, enabling the system to greatly enhance the free energy gain upon complexation, with respect to the case where no lipid mobility is allowed. This adds to the stability of the L_α^c complex. Generally, it was found that lipid mobility favors optimal (local) charge matching of the apposed DNA and lipid membrane. This is the state in which a maximal number of mobile counterions are expelled from the interaction zone, implying a maximal gain in free energy upon complex formation (126). However, the tendency for charge matching (hence migration of lipid to and from the region of proximity) is opposed by an unfavorable local lipid demixing entropy loss. This entropic penalty will somewhat suppress the membrane's tendency to polarize in the vicinity of the DNA molecule. The extent to which the membrane will polarize is determined by the intricate balance between the electrostatic and lipid-mixing entropy contributions to the free energy of the complex. The contribution of lipid demixing to the stabilization of the complex is most pronounced when the membrane's average composition is far from that of the DNA, namely, for low ϕ. Here, the system can gain most out of the polarization so as to come close to local charge matching.

The tendency of charged lipids to segregate in the vicinity of adsorbed rigid macromolecules has gained some experimental support from nuclear magnetic resonance (NMR) studies (127), although many systems may display a more complex behavior. Molecular dynamic simulations of L_α^c complexes, for a lipid mixture of DMTAP and DMPC, showed evidence for a favorable pairing of DMPC and DMTAP lipid molecules through the (partial) negative charge on DOPC, and an interaction of the (remaining) positive charge of the zwiterionic DOPC with the DNA. In contrast to the model discussed above, this implies a nonideal lipid demixing: these lipid molecules preferentially move in pairs (128). This may be anticipated because it is well known that lipids do not generally mix ideally, even in free (unassociated) membranes (129). Furthermore, there is evidence that to some extent neutral lipids also interact directly with DNA (133).

Figure 22 shows the experimental results and theoretical calculations for the dependence of d on ρ for several values of ϕ. For a specific value of ϕ (say $\phi = 0.5$), the 3-phase regimes can clearly be seen. As ρ increases, d changes from ≈ 35 Å (in the excess DNA regime, $\rho << 1$) to ≈ 47 Å (in the excess lipid regime, $\rho >> 1$). Both theory and experiment show that for a wide range of lipid composition, ϕ, there exists a 1-phase, complex-only region at ρ values somewhat larger and smaller than the isoelectric point. This implies that complexes may become either negatively or positively "overcharged," so that the total number of fixed positive and negative charges is not equal. Hence, the complex accommodates either an excess number of lipids or else an excess amount of DNA. The complex's free energy is thus not at its minimum, which occurs at isoelectricity ($\rho = 1$). The interplay between possible phases to minimize the total system's free energy dictates that the complex move away from its minimal free

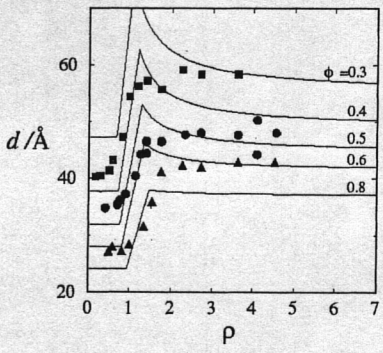

Figure 22 DNA–DNA spacing as a function of ρ in a series of theoretical and experimental results. The theoretical results correspond to (top to bottom) $\phi = 0.3$, 0.4, 0.5, 0.6, and 0.8; all results are presented for a screening length of 50 Å (corresponding to ca. 4 nm of bathing salt solution). The experimental results correspond to $\phi = 0.3$ (squares), 0.5 (circles), and 0.7 (triangles), and were performed with no added salt. (Theoretical results adapted from Refs. (125) and (145); experimental results adapted from Ref. 101.)

energy. The alternative would be to expel the excess lipid ($\rho > 1$) or excess DNA ($\rho < 1$) into solution. The charge densities on these "free" unneutralized macromolecules would be very large, rendering this scenario highly unfavorable. Using a simple model based on this overcharging phenomenon, it was possible to account for the considerable extent of this one phase region (125). Within this model, only the uncompensated charges on apposed (DNA–DNA or bilayer–bilayer) surfaces of an L_α^c unit cell ("box") were considered in estimating the complex's free energy. Figure 22 also shows that as the membrane becomes enriched in CL (ϕ increases) the DNA–DNA distance is systematically reduced, reflecting the fact that smaller amounts of lipid membrane are needed to achieve isoelectricity.

Salt has a significant effect on the phase behavior. In general, added salt causes a significant decrease in d, presumably due to a screening of the repulsive DNA–DNA interaction. This effect is most pronounced when divalent salts are added in increasing amounts. A sharp decrease in the d value is observed for a certain salt molar concentration, resulting in very highly condensed DNA in each gallery (89,130). Another interesting observation is that the identity of the CL's counterion used changes considerably the (endothermic) association enthalpy, particularly in the excess DNA region (121). This probably reflects the nonelectrostatic interaction energies of different ions with membranes, which may influence the thermotropic behavior of the lipid membranes (131,132).

D. DNA Adsorption on Lipid Membranes

Further insight into the in-plane DNA ordering in L_α^c complexes has been gained through the atomic force microscopy

(AFM) study by Fang and Yang (133,134) of DNA adsorption on supported lipid bilayers. In these experiments, DNA was first adsorbed on dipalmitoyldimethylammoniumylpropane (DPDAP) or distearoyl-DAP (DSDAP) CL bilayers, assumed to be in the gel phase. After equilibration and saturation of the surface, the DNA bulk solution was removed, and the surface was put in contact with solution of various concentrations of NaCl. After further equilibration, the salt solution was removed and the surface imaged by AFM. Plasmid and linear DNA similarly treated showed similar results.

Striking, fingerprint-like images of DNA adsorbed on the surface were revealed (Fig. 23). The typical domain size for the aligned, smecticlike order is usually several hundred Angstroms, reflecting the DNA's intrinsic persistence length. These structures are expected to be like those found in L_α^c complexes: the domain size, inferred from x-ray scattering is quite similar (103–104). Furthermore, it was found that the surfaces are often overcharged when DNA is adsorbed, (i.e., the number of DNA fixed charges exceeds the number of lipid charges). This can be anticipated on the basis of theoretical studies of a similar problem: adsorption of charged globular proteins (yet another macroion) on oppositely charged membranes (135). In both cases the driving force for adsorption is similar to that driving lipoplex formation, namely, counterion release. In L_α^c complex formation, much of the DNA can interact with the 2 sandwiching bilayers. In contrast, topology dictates that adsorbates on a single lipid bilayer will always possess a part proximal and a part distal to the interaction zone. If both parts are charged, as is the case with DNA, complete counterion release cannot be achieved because the distal part does not interact significantly with the underlying bilayer. Therefore, although charges on the lipid membrane are fully cancelled by charges on adsorbed DNA macroions, still the portion of DNA away from the contact zone imparts a net surface charge (i.e., overcharging of the DNA-covered membrane).

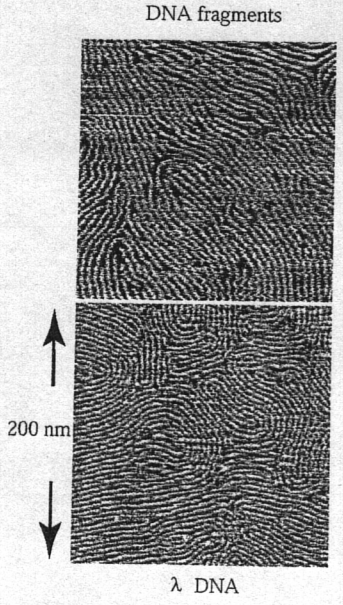

Figure 23 Atomic force microscopy images of DNA from different sources (see figure for details) condensed on DPDAP bilayers at room temperature in 20 mM NaCl. Striking fingerprint-like order is apparent, with a domain size of the order of the persistence length (ca. 50 nm). (Courtesy of J. Yang.)

Yet another interesting feature is the dependence of the DNA–DNA distance on salt concentration. As the NaCl concentration was varied between 20 and 1000 mM, this distance grew from around 45 Å to almost 60 Å. At first this may seem baffling: adding salt should be expected to decrease the DNA–DNA electrostatic repulsion, and hence lower the distance between neighboring interacting strands. This is indeed the general trend that has been observed in L_α^c complexes (101,125). However, because the DNA was primarily allowed to saturate the surface and only subsequently treated with the salt solution (which was later also washed away), adsorption here was not at equilibrium. In fact, when faced with a neat salt solution the adsorbed DNA can only detach, it will not generally readsorb onto the surface. It is therefore hard to give full theoretical reasoning for the trend.

Theoretical explanations have previously been offered to account for this salt-dependent behavior, based on a balance between membrane-mediated effective attraction (that may be the result of the DNA perturbation of the lipid bilayer) and electrostatic repulsion between DNA strands (136). The predicted DNA–DNA spacing as a function of screening length is nonmonotonic: increasing first for low screening lengths and decreasing for high values. An alternative to this approach is related to the free energy gain upon adsorption, and how it changes with the addition of salt. In the presence of added salt, the adsorption free energy can be expected to be lower because the gain in entropy upon release of counterions becomes very small when releasing an ion from an adsorbed layer into a bathing solution with a comparable concentration. Assuming that unbinding would occur when the free energy gain per persistence length is $\approx k_BT$, we can estimate from a simple model that the thickness of the confined layer is $l_{eff} \approx$ 5 Å, rather close to the screening length in solution (3–4 Å) (120–122). Thus, the lower binding free energy may cause some of the DNA strands to dissociate from the lipid surface once the system is exposed to salt. Allowing DNA to rearrange on the surface would then lead to an increase in the average DNA–DNA distance.

When multivalent salt is used, a crowding of DNA molecules is first observed as salt is added (in accordance with the observations in the L_α^c complexes), and then starts to grow for higher concentrations (89,137). This may be a manifestation of the 2 competing forces as salt is added: lessened repulsion between strands vs. weakened adsorption energy.

E. From Lamellar to Hexagonal Complexes

So far, we have discussed the L_α^c lipoplexes formed from lipid membranes that are rigid (bending rigidity much greater than

k_BT) and tend to a planar geometry. Other lipoplex structures may ensue when the lipids possess a spontaneous curvature that is nonplanar, or when the membranes are soft enough to be deformed under the influence of the apposed macroion. The lipid membrane thus responds to the presence of DNA by deforming elastically and by locally changing its composition ϕ.

Membrane elasticity may be varied substantially either by changing the lipid CL/HL composition, changing the lipid species, or by adding other agents, such as alcohols, to the membrane (138,139). In contrast, double-stranded DNA generally remains rather stiff, with a typical persistence length of $\approx$ 500 Å. Hence, the lipoplex geometries are restricted to structures in which DNA remains linear on these large-length scales. Usually, it is the interplay between the elastic (spontaneous curvature and bending rigidity) and electrostatic (charge density) properties of the membrane that will determine the optimum lipoplex geometry at equilibrium.

Often, the membrane elasticity and electrostatic contribution to the free energy display opposing tendencies. For example, the hexagonal H_{II}^c complex, is electrostatically favored due to the cylindrical wrapping of the DNA by the lipid monolayer. This allows better contact between the 2 macromolecular charged surfaces. However, the highly curved lipid geometry may incur a substantial elastic (curvature deformation) energy fee. The price to pay will be lower when the lipid (monolayer's) spontaneous curvature matches closely the DNA intrinsic (negative) curvature or when it has low bending rigidity. Under such conditions, the H_{II}^c complex may become more stable than the L_α^c phase. Usually, a neutral HL is used for adjusting the spontaneous curvature to the required negative curvature because pure CLs typically tend to form uncurved or positively curved aggregates. Use of more HL in the mixed membranes may on the one hand lower the elastic penalty, while on the other hand lower the monolayer's charge density, compromising the electrostatic energy gain upon association.

These qualitative notions were elegantly demonstrated by experiments in which the elastic properties of the lipid monolayers were controlled by changing the nature of the lipid mixture. The spontaneous curvature of the lipid bilayer was modified by changing the identity of HL. It was found that when using a mixture of DOTAP/DOPE, H_{II}^c was the preferred structure, while DOTAP/DOPC mixtures promoted the formation of the L_α^c phase. This is consistent with the fact that pure DOPE forms the inverted hexagonal phase, H_{II}, due to its high negative spontaneous curvature (140–142), while DOPC self-assembles into planar bilayer. In addition, by adding hexanol to the DOTAP/DOPC–DNA lipid mixture, the bending rigidity could be diminished by about 1 order of magnitude (138,139). This induced a clear first order $L_\alpha^c \rightarrow H_{II}^c$ phase transition (102).

Additional complexity can be expected when accounting for the coexistence of more than 1 phase in solution. A theoretical study of the phase equilibrium took into account the bare lipid phases L_α and H_{II}, the naked DNA and the complex L_α^c and H_{II}^c phases (143). The phase diagram of the system

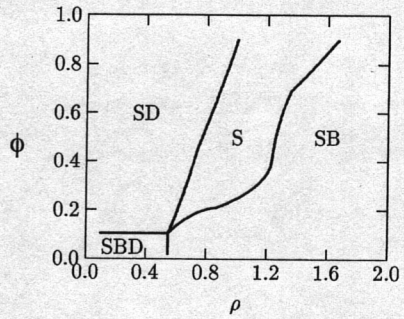

Figure 24 The phase diagram of a lipid–DNA mixture, for lipids that self-assemble into rigid planar membranes. The phase diagram was calculated for membranes characterized by a bending rigidity in the range of $4 < K_c < \infty$ k_BT and a spontaneous curvature of $c = 0$ Å^{-1} for both helper and cationic lipid. The symbols S, B, and D denote, respectively, the L_α^c, L_α, and uncomplexed (naked) DNA phases. (Reprinted by permission from Ref. 143, Biophysical Society.)

was evaluated by minimization of the total free energy, which included electrostatic, elastic, and lipid-demixing contributions. Several systems of different compositions were considered. Figure 24 shows the predicted phase coexistence corresponding to the simplest case already discussed of rigid planar membranes. Results are presented for lipid membranes with a bending rigidity of $K_c = 10k_BT$ per monolayer and spontaneous curvature $c = 0$ Å^{-1} [typical for many bilayer-forming lipids (106)] for which only lamellar complexes are expected to form. As the overall lipid composition is enriched in CL (higher ϕ) the 1 phase persists over a wider range of ρ. This indicates that for higher CL content, the complex may be expected to be more stable toward addition of either DNA or lipid (hence moving away from the isoelectric point).

The Gibbs phase rule allows for up to three phases to coexist concomitantly for this 3-component (DNA, HL and CL) system. Figure 25 shows the theoretical prediction for the phase diagram for a system in which the HL has a strong negative spontaneous curvature ($K_c = 10k_BT$ and $c = 1/25$ Å^{-1})(143). For high ϕ values, the phase behavior resembles that of the previously discussed system. However, for lower values of ϕ, a multitude of regions of (up to 3) different phases coexisting together can be found. In some regions, lamellar and hexagonal complexes appear coexisting side by side. A similarly complex diagram results when the membranes are soft (bending rigidity of $\approx k_BT$) as might be expected for membranes with added alcohols (143).

A more subtle demonstration of the underlying balance of forces can be found within the realm of the L_α^c complex. Thus far, the theoretical models considered for the lipid membranes in this lamellar phase assumed them to be perfectly planar slabs. However, this need not be so. When membranes are sufficiently soft (yet not soft enough to favor the H_{II}^c phase) or if one of the CL/HL has a propensity to form curved sur-

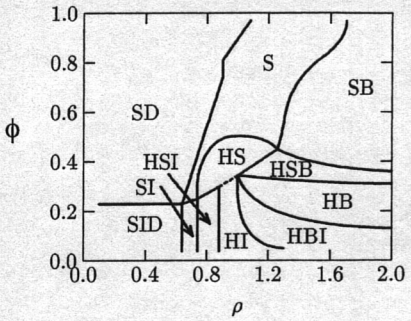

Figure 25 The phase diagram of a lipid–DNA mixture involving "curvature-loving" helper lipid. The spontaneous curvature of the helper lipid is $c = -1/25$ Å^{-1}. For the cationic lipid, the spontaneous curvature taken is $c = 0$ Å^{-1}. The bending rigidity for both lipids is $K_c = 10\ k_BT$. The symbols *S*, *H*, *B*, *I*, and *D* denote, respectively, the L_α^c, H_{II}^c, L_α, H_{II}, and uncomplexed (naked) DNA phases. The broken line marks the single H_{II}^c phase. (Reprinted by permission from Ref. 143, Biophysical Society.)

faces, the membrane may corrugate so as to optimize its contact with DNA (see Fig. 19A). If the membrane is further softened, finally, a transition may occur to the H_{II}^c phase. In this respect, the membrane corrugation in the L_α^c complex may be regarded as a further stabilization of the lamellar complex, and a delay to the onset of the $L_\alpha^c \rightarrow H_{II}^c$ transition.

A possible consequence of membrane corrugation in the L_α^c phase is an induced locking between neighboring galleries. This follows the formation of "troughs" in a gallery, induced by the interaction of the membrane with DNA in adjacent galleries. This imposes "adsorption sites" for the DNA in the 2 neighboring galleries, which propagates the order on. The formation of these troughs, as well as a very weak electrostatic interaction between galleries, may thus correlate between the positions of DNA in different galleries (128,144,145). Limited experimental evidence supports this notion. In cryotransmission electron microscopy (cryo-TEM) studies of the L_α^c phase, spatial correlations were found between DNA strands in different galleries (146). In another series of X-ray studies, the corrugation and charge density modulation in an L_α^c-like complex, in which the membranes are in the gel phase, were measured (147). Further support for the possible formation of corrugations is gained from computer simulations of lipid–DNA complexes (128).

In order to assess the extent of membrane corrugation, a balance of forces between many degrees of freedom should be taken into account. The free energy minimum now depends on the local membrane composition—dictating membrane properties such as local charge density, spontaneous curvature and bending elasticity—and the extent of local deformation around the DNA. Theoretical predictions show that for a wide range of conditions, both stiff and soft membranes can show corrugations that are stable with respect to thermal undulations of the membranes (145). The spacings between galleries and between DNA molecules are also predicted to change somewhat with respect to the case where no corrugations are allowed (144). For the conditions in which the troughs are shallow or absent altogether, one may anticipate the formation of phases where DNA in different galleries are positionally uncorrelated, while orientational order is preserved. These structures were predicted theoretically and termed "sliding phases" (103,104,148–150,146).

F. Lipoplex Structure and Transfection Efficiency

In recent years a large number of CL–DNA formulations have been proposed as vectors. However, the fate of the CL–DNA complex once administered, its interaction with the cell membrane, and entry into the cell and subsequently into the cell nucleus, is likely complex and largely unresolved. The poorly understood process of DNA release once in the cell interior must be important (151–153). For example, it has been shown from action in the nucleus that DNA expression is diminished when it is tightly complexed with lipids (156). Hints to the mechanism of the intracellular release of lipoplexes come from experimental evidence in vitro, showing that other added polyelectrolytes may compete with DNA and subsequently replace it in the complex (154). This kind of replacement, by natural polyelectrolytes, may be one way in which DNA is released in cells (155). Another possible mechanism is the fusion of complex lipids with lipid membranes in the cell (89,104).

Only a limited number of experiments have probed the relationship between the structure of CL–DNA complexes and the transfection efficiency. One emergent theme attributes an important role to complex frustration and destabilization in promoting transfection.

Experimental studies show that the 2 ordered complex structures, L_α^c and H_{II}^c, behave differently inside living cells. Furthermore, a correlation was found between the structure of the lipoplexes formed and the transfection efficiency. The structure formed depends in turn on the specific choice and relative amount of HL, CL, and DNA. The H_{II}^c complex was found (in the studied cases) to be a more potent vector than L_α^c (157). Further information is gained from fluorescence studies of cell cultures with both complex types internalized in fibroblast L cells. These indicate that the L_α^c complex is more stable inside the cells, while the H_{II}^c more readily disintegrates—its lipids fusing with the cell's own (endosomal or plasma) membranes—resulting in DNA release. This is in accord with the theoretical findings that the L_α^c complex structure is rather flexible toward changes in the system's compositional parameters, due to its ability to tune both the membrane composition and the DNA–DNA spacing, while this tuning is more limited in the H_{II}^c phase.

The picture is further substantiated by a series of studies by Barenholtz and coworkers (90,152,153,158). In general it was shown that maximal transfection efficiency could be achieved in complexes that were formed in the excess lipid regime (with ρ in the range of 2–5). This correlated well with the point of maximal size heterogeneity of the complexes.

These instabilities were shown to occur concomitantly with an increase in the amount of membrane defects that were in turn mainly attributed to the appearance of several coexisting structures in solution (e.g., H_{II}^{c} and L_{α}^{c} in DOTAP/DOPE lipoplexes, or micellar and lamellar phases in DOSPA/DOPE-based lipoplexes). This is in accordance with the theoretical prediction that the regions of most phase diversity and the largest number of coexisting phases occurs at high ρ (and low ϕ) values (see Fig. 25) (90,114,140).

Other evidence seems to agree with these notions. For example, some successful formulations, such as BIV, are also probably metastable (97,99,110). This may suggest that it is in fact their instability that helps them to release their DNA cargo once they are inside the cell. Attempts have also been made to destabilize lipoplexes more specifically only once they are already internalized in the cells (rather than en route in the serum). Reduction-sensitive cationic lipids were designed, and the subsequent lipoplexes that are formed were shown to undergo large structural changes when exposed to the cytoplasmic reductive systems. The lipoplexes are thus destabilized and the previously packaged DNA is released into the cytosol (92,159–161). A decrease in the toxicity of the CL and increased transfection efficiency are thus achieved (162).

Destabilizing lipoplexes is not the only barrier to transfection. For example, entry of DNA into the nucleus through the nuclear pore complex is inefficient for large pieces of DNA. It has been shown that the cell own nuclear import machinery may be used to increase transfection efficiency dramatically, by attaching a peptide containing a nuclear localization signal (NLS) to the DNA (163,164). Furthermore, the size of the complexes also seems to play a crucial role in determining transfection efficiencies (90,91,97,99). Here, the repulsive interaction between like-surface charge of the complex due to over/undercharging (excess lipid or DNA) can aid in stabilizing the complexes, once they are formed, from fusing further. Another strategy to controlling the interaction between aggregates and the stability of the aggregate in vivo is to modify the composition of the outer wrapping sheath of the lipoplex. The caveat is that the lipoplexes are not stabilized to such a degree that they can no longer disintegrate once inside the cells. For example, short-chain lipids possessing a PEG headgroup (or a derivative thereof) have been used to increase the stability of the lipoplexes in the bloodstream, while not interfering with the endosomal unwrapping once the lipoplexes are internalized in cells (165).

More generally, we can expect that understanding how to control and manipulate the formation of specific phases on the one hand, while better understanding the multistage transfection mechanism and the parameters (conditions) affecting it on the other, should aid in the design of more potent lipid-based gene delivery vectors in the future. These, together with control over the coating and targeting of the complexes, may render these vectors as useful vehicles in gene therapy.

VI. RETROSPECT AND PROSPECT

Structural elucidation of the DNA–cationic lipid complexes and realization of the extent to which they share the structural features of pure DNA or pure lipid polymorphism have advanced notably in the past few years. Some old questions have been answered and new questions raised. It is these new questions that challenge our knowledge of the intricacies of interactions between macromolecules.

The DNA–lipid complexes found so far are only a sample of the much wider set of structures that will be seen on a full DNA–lipid phase diagram. We argue that this larger set of possibilities be approached by firmly established methods to measure the energies of these structures at the same time that they are determined and located on a phase diagram. Built on principles of direct molecular interactions, recognizing the consequences of thermal agitation, this line of observation and analysis can lead to an understanding of the energetic ''whys'' and preparative ''hows'' of complex structures.

Forces so delineated are already knowledgeably applied in new preparations. Precisely how the structure of DNA–lipid aggregates will affect their efficacy in transfection remains to be seen. So far, the ideas we have are too general and have been learned from studying analytically tractable but technically inadequate preparations. General principles do not lead to specific results. Molecules are too interesting to allow easy success in clinical design. Still there is little doubt of a practical link between the energy and structure of these complexes and their viability in a technological application.

Even the present general understanding of forces, even the cartoon ideas of the directions in which forces act in macromolecular complexes can tutor the bench scientist on how to improve preparations. There is enough known for a healthy iteration between experimental attempt and theoretical reason. Experimental successes and failures become the data for molecule force analyses. Various DNA–lipid assemblies reflect the various actions of competing forces. Molecular theorists can define and delineate these forces as they act to create each form; they can provide a logic to design variations in preparation. Basic scientists and clinicians are already in a position to help each other to improve their ways.

ACKNOWLEDGMENTS

We want to thank Milan Hodoscek for his help with molecular graphics in preparing some of the figures. We also want to thank John Nagle and Stephanie Tristram-Nagle for their comments on an earlier version of this chapter.

REFERENCES

1. Bloomfield VA, Crothers DM, Tinoco I. Nucleic Acids: Structures, Properties and Functions: Mill Valley: University Science Books, 1998.
2. Vologotskii AV. Topology and Physics of Circular DNA (Physical Approaches to DNA): Boca Raton, FL: CRC Press, 1992.
3. Strey HH, Podgornik R, Rau DC, Parsegian VA. Colloidal DNA. Curr Op Coll Interf Sci 1998; 3:534–539.
4. Podgornik R, Strey HH, Parsegian VA. DNA–DNA interactions. Curr Opin Struct Biol 1998; 8:309–313.

5. Kabanov VA, Flegner P, Seymour LW. Self-assembling complexes for gene delivery: John Wiley & Sons, 1998.
6. Lasic DD. Liposomes in Gene Delivery: >Boca Raton, FL: CRC Press, 1997.
7. Podgornik R, Rau DC, Parsegian VA. Parametrization of direct and soft steric-undulatory forces between DNA double helical polyelectrolytes in solutions of several different anions and cations. Biophys. J 1994; 66:962–971.
8. Livolant F, Leforestier A. DNA mesophases. A structural analysis in polarizing and electron microscopy. Mol Cryst Liq Cryst 1992; 215:47–56.
9. Derjaguin BV, Churaev NV, Muller VM. Surface Forces. New York: Plenum, 1987.
10. Bloomfield VA. DNA condensation. Curr Opin Struc Biol 1996; 6:334–341.
11. Leikin S, Parsegian VA, Rau DC, Rand RP. Hydration forces. Annu Rev Phys Chem 1993; 44:369–395.
12. Darnell J, Lodish H, Baltimore D. Molecular Cell Biology. New York: Scientific American Books, 1990.
13. Cerritelli ME, Cheng N, Rosenberg AH, McPherson CE, Booy FP, Steven AC. Encapsidated conformation of bacteriophage T7 DNA. Cell 1997; 91:271–280.
14. Safinya CR, Koltover I, Rädler J. DNA at membrane surfaces: An experimental overview. Curr Opin Colloid Interf Sci 1998; 1:69–77.
15. Mahanty J, Ninham BW. Dispersion Forces. London: Academic Press, 1976.
16. Safran SA. Statistical Thermodynamics of Surfaces, Interfaces and Membranes. New York: Addison Wesley, 1994.
17. Eisenberg D, Kauzmann W. The Structure and Properties of Water. Oxford: Clarendon Press, 1969.
18. Parsegian VA, Rand RP, Fuller NL, Rau DC. Osmotic stress for the direct measurement of intermolecular forces. Methods Enzymol 1986; 127:400–416.
19. Marčelja S, Radić N. Repulsion of interfaces due to boundary water. Chem Phys Lett 1976; 42:129–130.
20. Rand RP, Parsegian VA. Hydration forces between phospholipid bilayers. Biochim Biophys Acta 1989; 988:351–376.
21. Kornyshev AA, Leikin S. Fluctuation theory of hydration forces: The dramatic effects of inhomogeneous boundary conditions. Phys. Rev. A 1998; 40:6431–6437.
22. Rau DC, Parsegian VA. Direct measurement of the intermolecular forces between counterion-condensed DNA double helices: Evidence for long range attractive hydration forces. Biophys J 1992; 246–259.
23. Parsegian VA. Long-range physical forces in the biological milieu. Ann Rev Biophys Bioeng 1973; 2:221–255.
24. Bernal JD, Fankuchen I. X-ray and crystallographic studies of plant virus preparations. J. Gen Physiol 1942; 25:111–165.
25. Verwey EJW, Overbeek JTG. Theory of the Stability of Lyophobic Colloids. New York: Elsevier, 1948.
26. Hill TL. Statistical Mechanics. Principles and Selected Applications. New York: Dover, 1956.
27. Andelman D. Electrostatic properties of membranes: The Poisson–Boltzmann theory. In: Lipowsky R, Sackmann E, Eds. Structure and Dynamics of Membranes. Vol. 1B. Amsterdam: Elsevier, 1995:603–642.
28. Landau LD, Lifshitz EM. The Classical Theory of Fields. 4th ed.: Butterworth-Heinemann, 1986.
29. McLaughlin S. Electrostatic potential at membrane solution interfaces. Curr Top Membr Transp 1985; 4:71–144.
30. Brenner SL, McQuarrie DA. Force balances in systems of cylindrical polyelectrolytes. Biophys J 1973; 13:301–331.
31. Parsegian VA, Rand RP, Fuller NL. Direct osmotic stress measurements of hydration and electrostatic double-layer forces between bilayers of double-chained ammonium acetate surfactants. J Phys Chem 1991; 95:4777–4782.
32. Kjellander R. Ion-ion correlations and effective charges in electrolyte and macroion systems. Ber Bunsenges Phys Chem 1996; 100:894–904.
33. Hunter RJ. Foundations of Colloid Science. New York: Oxford University Press, 1987.
34. Parsegian VA. Long range van der Waals forces. In: van Olphen H, Mysels KL, Eds. Physical Chemistry: Enriching Topics from Colloid and Interface Science, 1975:27–72.
35. Landau LD, Lifshitz EM. Statistical Physics Part 2: Butterworth-Heinemann, 1986.
36. Parsegian VA, Rand RP. Interaction in membrane assemblies. In: Lipowsky R, Sackmann E, Eds. Structure and Dynamics of Membranes. Vol. 1B. Amsterdam: Elsevier, 1995:643–690.
37. Parsegian VA. Non-retarded van der Waals between anisotropic long thin rods at all angles. J Chem Phys 1972; 56: 4393–4397.
38. Brenner SL, Parsegian VA. A physical method for deriving the electrostatic interaction between rod-like polyions at all mutual angles. Biophys J 1974; 14:327–334.
39. Parsegian VA, Fuller N, Rand RP. Measured work of deformation and repulsion of lecithin bilayers. Proc Natl Acad Sci. USA 1979; 76:2750–2754.
40. Lipowsky R. Generic interactions of flexible membranes. In: Lipowsky R, Sackmann E, Eds. Structure and Dynamics of Membranes. Vol. 1B. Amsterdam: Elsevier, 1995:521–596.
41. Helfrich W. Steric interactions of fluid membranes in multilayer systems. Z Naturforsch 1978; 33a:305–315.
42. Strey HH, Parsegian VA, Podgornik R. Equation of state for polymer liquid crystals: Theory and experiment. Phys Rev E 1998; 59:999–1008.
43. Seifert U, Lipowsky R. Morphology of vesicles. In: Lipowsky R, Sackmann E, Eds. Structure and Dynamics of Membranes. Vol. 1A. Amsterdam: Elsevier, 403.
44. Podgornik R, Parsegian VA. Thermal—Mechanical fluctuations of fluid membranes in confined geometries: The case of soft confinement. Langmuir 1992; 8:557–562.
45. Podgornik R, Parsegian VA. Charge-fluctuation forces between rodlike polyelectrolytes: Pairwise summability reexamined. Phys Rev Lett 1998; 80:1560–1563.
46. Ha BJ, Liu AJ. Counterion-mediated attraction between two like charged rods. Phys Rev Lett 1997; 79:1289–1292.
47. Saenger W. Principles of Nucleic Acid Structure, Springer Verlag. 1984.
48. Rhodes D, Klug A. Helical periodicity of DNA determined by enzyme digestion. Nature 1980; 286:573–578.
49. Rill RL. Liquid crystalline phases in concentrated DNA solutions. In: Pifa-Mrzljak G, Ed. Supramolecular Structure and Function. New York: Springer, 1988:166–167.
50. De Gennes PG, Prost J. The Physics of Liquid Crystals. 2nd ed.. Oxford: Oxford University Press, 1993.
51. Hagerman PJ. Flexibility of DNA. Ann Rev Biophys Biophys Chem 1988; 17:265–286.
52. Pruss GJ, Drlica K. DNA supercoiling and prokaryotic transcription. Cell 1989; 56:521–523.
53. Grosberg AY, Khokhlov AR. Statistical Physics of Macromolecules (AIP Series in Polymers and Complex Materials): American Institute of Physics, 1994.
54. Rau DC, Lee BK, Parsegian VA. Measurement of the repulsive force between polyelectrolyte molecules in ionic solution: Hydration forces between parallel DNA double helices. PNAS 1984; 81:2621–2625.
55. Strey HH, Parsegian VA, Podgornik R. Equation of state for DNA liquid crystals: Fluctuation enchanced electrostatic double layer repulsion. Phys Rev Lett 1997; 78:895–898.

56. Reich Z, Wachtel EJ, Minsky A. In vivo quantitative characterization of intermolecular interaction. J Biol. Chem 1995; 270: 7045–7046.
57. Barrat JL, Joanny JF. Theory of polyelectrolyte solutions. In: Prigogine I, Rice SA, Eds. Advances in Chemical Physics. New York: John Wiley & Sons, 1995:1–66.
58. Lyubartsev AP, Nordenskiold L. Monte Carlo simulation study of ion distribution and osmotic pressure in hexagonally oriented DNA. J Phys Chem 1995; 99:10373–10382.
59. Oosawa F. Polyelectrolytes. New York: Marcel Dekker, 1971.
60. Rouzina I, Bloomfield VA. Macro-ion Attraction due to Electrostatic Correlation between Screening Counterions. J Phys Chem 1996; 100:9977–9989.
61. Podgornik R, Strey HH, Rau DC, Parsegian VA. Watching molecules crowd: DNA double helices under osmotic stress. Biophys Chem 1995; 26:111–121.
62. Lindsay SM, Lee SA, Powell JW, Weidlich T, Demarco C, Lewen GD, Tao NJ, Rupprecht A. The origin of the A to B transition in DNA fibers and films. Biopolymers 1988; 17: 1015–1043.
63. Podgornik R, Strey HH, Gawrisch K, Rau DC, Rupprecht A, Parsegian VA. Bond orientational order, molecular motion, and free energy of high-density DNA mesophases. Proc Natl Acad Sci USA 1996; 93:4261–4266.
64. Strandberg D. Bond-Orientational Order in Condensed Matter Systems. New York: Springer, 1992.
65. Durand D, Doucet J, Livolant F. A study of the structure of highly concentrated phases of DNA by X-ray diffraction. J. Phys. II France 1992; 2:1769–1783.
66. Kamien RD. Liquids with chiral bond order. J. Phys. II France 1996; 6:461–475.
67. Chaikin PM, Lubensky TC. Principles of condensed matter physics. Cambridge: Cambridge University Press, 1995.
68. Leforestier A, Livolant F. DNA liquid-crystalline blue phases—Electron-microscopy evidence and biological implications. Mol Cryst Liquid Cryst 1994; 17:651–658.
69. Wang L, Bloomfield VA. Small-angle X-ray scattering of semidilute rodlike DNA solutions: Polyelectrolyte behavior. Macromolecules 1991; 24:5791–5795.
70. Podgornik R, Rau DC, Parsegian VA. The action of interhelical forces on the organization of DNA double helices: Fluctuation enhanced decay of electrostatic double layer and hydration forces. Macromolecules 1989; 22:1780–1786.
71. Frank-Kamenetskii MD, Anshelevich VV, Lukashin AV. Polyelectrolyte model of DNA. Sov Phys Usp 1987; 4:317–330.
72. Tanford C. The Hydrophobic Effect. Formation of Micelles and Biological Membranes. New York: John Wiley & Sons, 1980.
73. Cevc G, Marsh D. Phospholipid bilayers: Physical principles and models Cell Biology: A Series of Monographs. Vol. 5, 1987.
74. Parsegian VA, Evans EA. Long and short range intermolecular and intercolloidal forces. Curr Opin Coll Interf Sci 1996; 1: 53–60.
75. Duzgunes N, Willshut L, Hong K, Fraley R, Perry C, Friends DS, James TL, Papahadjopoulos D. Physicochemical characterization of large unilamelar phospholipid vesicles prepared by reverse-phase evaporation. Biophys. Biochim. Acta 1983; 732:289–299.
76. Seifert U. Configurations of fluid membranes and vesicles. Adv Phys 1997; 46:13–137.
77. Small DM. The Physical Chemistry of Lipids. From Alkanes to Phospholipids. New York: Plenum Press, 1986.
78. Gruner SM, Parsegian VA, Rand RP. Directly measured deformation energy of phospholipid H2 hexagonal phases. Faraday Disc 1986; 81:213–221.
79. Daoud M, Williams CE. Soft Matter Physics. New York: Springer, 1999.
80. Lasic DD. Liposomes: From Physics to Applications. Amsterdam: Elsevier, 1993.
81. Parsegian VA, Podgornik R. Surface-tension suppression of lamellar swelling on solid substrates. Colloids Surf. A Physicochem. Eng. Asp 1997; 129–130:345–364.
82. Roux D, Safinya CR. A synchrotron X-ray study of competing undulation and electrostatic interlayer interactions in fluid multimembrane lyotropic phases. J Phys—Paris 1988; 49: 307–318.
83. Leneveu DM, Rand RP, Gingell D, Parsegian VA. Apparent modification of forces between lecithin bilayers. Science 1976; 191:399–400.
84. Parsegian VA. Reconciliation of van der Waals force measurements between phosphatidylcholine bilayers in water and between bilayer coated mica surfaces. Langmuir 1993; 9: 3625–3628.
85. Gouliaev N, Nagle JF. Simulations of interacting membranes in soft confinement regime. Phys Rev Lett 1998; 81: 2610–2613.
86. Rand RP, Parsegian VA. Hydration forces between phospholipid bilayers. Biochim Biophys Acta 1989; 988:351–376.
87. Petrache HI, Gouliaev N, Tristram-Nagle S, Zhang R, Suter RM, Nagle JF. Interbilayer interactions from high-resolution X-ray scattering. Phys Rev E 1998; 57:7014–7024.
88. Felgner PL, Barenholz Y, Behr JP. Nomenclature for synthetic gene delivery systems. Hum Gene Ther 1997; 8:511–512.
89. Safinya CR. Structure of lipid-DNA complexes: Supermolecular assembly and gene delivery. Curr Op Struc Biol 2001; 11: 440–448.
90. Barenholz Y. Liposome application: Problems and prospects. Curr Opin Coll Inter Sci 2001; 6:66–77.
91. Rädler JO. Structure and phase behavior of cationic-lipid DNA complexes. In: Holm C, Kékicheff P, Podgornik R, Eds. Electrostatic effects in soft matter and biophysics. Dordrecht: Kluwer, 2001:441–458.
92. Ilies MA, Balaban AT. Recent developments in cationic lipid-mediated gene delivery and gene therapy. Expert Opin Ther Patents 2001; 11:1729–1751.
93. Ilies MA, William AS, Balaban AT. Cationic lipids in gene delivery: Principles, vector design and therapeutical applications. Curr Pharm Des 2002; 8:125–133.
94. Audouy S, Hoekstra D. Cationic-mediated transfection in vitro and in vivo. Mol Membr Biol 2001; 18:129–143.
95. Felgner PL, Gadeck T, Holen M. Lipofectin: a highly efficient lipid-mediated DNA transfection procedure. Proc Natl Acad Sci USA 1987; 84:7413–7417.
96. Felgner PL, Ringold GM. Cationic liposome-mediated transfection. Nature 1989; 337:387–388.
97. Tempelton NS. Developments in liposomal gene delivery systems. Expert Opin Biol Ther 2001; 1:1–4.
98. Fraley R, Subramani S, Berg P, Papahadjopoulos D. Introduction of liposome-encapsulated SV40 DNA into cells. J Biol Chem 1980; 255:10431–10435.
99. Lasic DD, Templeton NS. Liposomes in gene therapy. Adv Drug Deliv Rev 1996; 20:221–266.
100. Lasic DD, Strey H, Stuart MCA, Podgornik R, Frederik PM. The structure of DNA–liposome complexes. J Am Chem Soc 1997; 119:832–833.
101. Rädler JO, Koltover I, Salditt T. Structure of DNA–cationic liposome complexes: DNA intercalation in multilamellar membranes in distinct interhelical packing regimes. Science 1997; 275:810–814.
102. Koltover I, Salditt T, Rädler JO. An inverted hexagonal phase of cationic liposome–DNA complexes related to DNA release and delivery. Science 1998; 281:78–81.

103. Salditt T, Koltover I, Rädler O. Self-assembled DNA–cationic–lipid complexes: Two-dimensional smectic ordering, correlations, and interactions. Phys Rev E 1998; 58:889–904.
104. Salditt T, Koltover I, Rädler J, Safinya CR. Two dimensional smectic ordering of linear DNA chains in self-assembled DNA–cationic liposome mixtures. Phys Rev Lett 1997; 79: 2582–258.
105. Rädler JO, Koltover I, Jamieson A, Salditt T, Safinya CR. Structure and interfacial aspects of self-assembled cationic lipid–DNA gene carrier complexes. Langmuir 1998; 14: 4272–4283.
106. Sackmann E. Physical basis of self-organization and function of membranes: Physics of vesicles. In: Lipowsky R, Sackmann E, Eds. Structure and Dynamics of Membranes. Amsterdam: Elsevier, 1995:213–304.
107. Tarahovsky YS, Khusainova RS, Gorelov AV. DNA initiates polymorphic structural transitions lecithin. FEBS Lett 1996; 390:133–136.
108. Ghirlando R, Wachtel EJ, Arad T, Minsky A. DNA packaging induced by micellar aggregates: A novel in vitro DNA condensation system. Biochemistry 1992; 31:7110–7119.
109. Gershon H, Ghirlando R, Guttman SB, Minsky A. Mode of formation and structural features of DNA–cationic liposome complexes used for transfection. Biochemistry 1993; 32: 7143–7151.
110. May S, Ben-Shaul S. DNA–lipid complexes: Stability of honeycomb-like and spaghetti-like structures. Biophys J 1997; 73:2427–2440.
111. Dan N. The structure of DNA complexes with cationic liposomes—Cylindrical or lamellar, Biophys Biochim Acta 1998; 1369:34–38.
112. Sternberg B, Sorgi FL, Huang L. New structures in complex-formation between DNA and cationic liposomes visualized by freeze-fracture electron-microscopy. FEBS Lett 1994; 356: 361–366.
113. Sternberg B. New structures in complex formation between DNA and cationic liposomes visualized by freeze-fracture electron microscopy. FEBS Lett 1994; 356:361–366.
114. Simberg D, Danino D, Talmon Y, Minsky A, Ferrari ME, Wheeler CJ, Barenholz Y. Phase behaviour, DNA ordering, and size instability of cationic lipoplexes. J Biol Chem 2001; 276:47453–47459.
115. Pitard B, Aguerre O, Airiau M, Lachages AM. Virus-sized self-assembling lamellar complexes between plasmid DNA and cationic micelles promote gene transfer. Proc Natl Acad Sci USA 1997; 94:14412–14417.
116. Boukhnikashvili T, Aguerre-Chariol O, Airiau M, Lesieur S, Ollivon M, Vacus J. Structure of in-serum transfecting DNA–cationic lipid complexes. FEBS Lett 1997; 409: 188–194.
117. Templeton NS, Lasic DD, Frederik PM, Strey HH, Roberts DD, Pavlakis GN. Improved DNA: Liposome complexes for increased systemic delivery and gene expression. Nat Biotech 1997; 15:647–652.
118. Record TM, Anderson CF, Lohman TM. Thermodynamic analysis of ion effects on the binding and conformational equilibria of proteins and nucleic acids: The roles of ion association or release, screening, and ion effects on water activity. Q Rev Biophys 1978; 11:103–178.
119. Bruinsma R. Electrostatics of DNA-cationic lipid complexes: Isoelectric instability. Eur. Phys. J. B 1998; 4:75–88.
120. Wagner K, Harries D, May S. Counterion release upon cationic lipid-DNA complexation. Langmuir 2000; 16:303–306.
121. Barreleiro PCA, Olofsson G, Alexandridis P. Interaction of DNA with cationic vesicles: a calorimetric study. J. Phys. Chem. B 2000; 104:7795–7802.
122. Kennedy MT, Pozharski EV, Rakhmanova VA, MacDonald RC. Factors governing the assembly of cationic phospholipid–DNA complexes. Biophys J 2000; 78:1620–1633.
123. Huebner S, Battersby BJ, Grimm R, Cevc G. Lipid mediated complex formation: Reorganization and rupture of lipid vesicles in the presence of DNA as observed by cryoelectron microscopy. Biophys J 1999; 76:3158–3166.
124. Dan N. Multilamellar structures of DNA complexes with cationic liposomes. Biophys J 1997; 73:1842–1846.
125. Harries D, May S, Gelbart WM, Ben-Shaul A. Structure, stability and thermodynamics of lamellar DNA–lipid complexes. Biophys J 1998; 75:159–173.
126. Parsegian VA, Gingell D. On the electrostatic interaction across a salt solution between two bodies bearing unequal charges. Biophys J 1972; 12:1192–1204.
127. Mitrakos P, Macdonald PM. DNA-induced lateral segregation of cationic amphiphiles in lipid bilayer membranes as detected via ^{2}H NMR. Biochemistry 1996; 35:16714–16722.
128. Bandyopadhyay S, Tarek M, Klein ML. Molecular dynamics study of a lipid–DNA complex. J Phys Chem B 1999; 103: 1007–1008.
129. Garidel P, Johann C, Blume A. Thermodynamics of lipid organization and domain formation in phospholipid bilayers. J Liposome Res 2000; 10:131–158.
130. Koltover I, Wagner K, Safinya CR. DNA condensation in two dimensions. PNAS 2000; 97:14046–14051.
131. Dubois M, Zemb Th, Fuller N, Rand RP, Parsegian VA. Equation of state of a charged bilayer system: Measure of the entropy of the lamellar–lamellar transition in DDABr. J Chem Phys 1998; 18:7855–7869.
132. Bostrom M, Williams DRM, Ninham B. Specific ion effects: Why DLVO theory fails. Phys Rev Lett 2001; 87: 168103–1–4.
133. Fang Y, Yang J. Two-dimensional condensation of DNA molecules on cationic lipid membranes. J Phys Chem B 1997; 101:441–449.
134. Mou J, Czajkowsky DM, Zhang Y, Shao Z. High-resolution atomic force microscopy of DNA: The pitch of the double helix. FEBS Lett 1995; 371:279–282.
135. May S, Harries D, Ben-Shaul A. Lipid demixing and protein–protein interactions in the adsorption of charged proteins on mixed membranes. Biophys J 2000; 79:1747–1760.
136. Dan N. Formation of ordered domains in membrane-bound DNA. Biophys J 1996; 71:1267–127.
137. Fang Y, Yang J. Effect of cationic strength and species on 2-D condensation of DNA. J Phys Chem B 1997; 101:3453–3456.
138. Safinya CR, Sirota EB, Roux D, Smith GS. Universality in interacting membranes: The effect of cosurfactants on the interfacial rigidity. Phys Rev Lett 1989; 62:1134–1137.
139. Szleifer I, Kramer D, Ben-Shaul A, Roux D, Gelbart MW. Curvature elasticity of pure and mixed surfactant films. Phys Rev Lett 1998; 60:1966–1969.
140. Gawrisch K, Parsegian VA, Hajduk DA, Tate MW, Gruner SM, Fuller NL, Rand RP. Energetics of a hexagonal-lamellar-hexagonal-phase transition sequence in dioleoylphosphatidylethanolamine membranes. Biochemistry 1992; 31: 2856–2864.
141. Kozlov MM, Leikin S, Rand RP. Bending, hydration and interstitial energies quantitatively account for the hexagonal-lamellar-hexagonal reentrant phase transition in dioleoylphosphatidylethanolamine. Biophys J 1994; 67:1603–1611.
142. Chen Z, Rand RP. Comparative study of the effects of several n-alkanes on phospholipid hexagonal phases. Biophys J 1998; 74:944–952.
143. May S, Harries D, Ben-Shaul A. The phase behavior of cationic lipid–DNA complexes. Biophys. J 2000; 78: 1681–1697.

144. Schiessel H, Aranda-Espinoza H. Electrostatically induced undulations of lamellar DNA–lipid complexes. Eur Phys J E 2001; 5:499–506.
145. Harries D. Electrostatic interaction between macromolecules and mixed lipid membranes. Ph.D. dissertation/~/. Jerusalem. Israel: The Hebrew University, 2001.
146. Battersby BJ, Grimm R, Huebner S, Cevc G. Evidence for three-dimensional interlayer correlations in cationic lipid–DNA complexes as observed by cryo-electron microscopy. Biochim Biophys Acta 1998; 1372:379–383.
147. Artzner F, Zantl R, Rapp G, Rädler JO. Observation of a rectangular columnar phase in condensed lamellar cationic lipid–DNA complexes. Phys Rev Lett 1998; 81:5015–5018.
148. O'Hern CS, Lubensky TC. Sliding columnar phase of DNA lipid complexes. Phys Rev Lett 1998; 80:4345–4348.
149. Golubovic L, Golubovic M. Fluctuations of quasi-two-dimensional smectics intercalated between membranes in multilamellar phases of DNA cationic lipid complexes. Phys Rev Lett 1998; 80:4341–4344.
150. Podgornik R, Žekš B. Coupling between smectic and twist modes in polymer intercalated smectics. Phys Rev Lett 1998; 80:305–308.
151. Hui SW, Langner M, Zhao Y-L, Patrick R, Hurley E, Chan K. The role of helper lipids in cationic liposome-mediated gene transfer. Biophys J 1996; 71:590–59.
152. Zuidam NJ, Lerner DH, Margulies S, Barenholz Y. Lamellarity of cationic liposomes and mode of preparation of lipoplexes affect transfection efficiency. Biophys Biochim Acta 1999; 1419:207–220.
153. Meidan VM, Cohen JS, Amariglio N, Hirsch-Lerner D, Barenholz Y. Interaction of oligonucleotides with cationic lipids: the relationship between electrostatics, hydration and state of aggregation. Biochem Biophys Acta 2000; 1464:251–261.
154. Artzner F, Zantl R, Rädler JO. Lipid-DNA and lipid-polyelectrolyte mesophases: Structure and exchange kinetics. Cell Molec Biol 2000; 46:967–978.
155. Wiethoff CM, Smith JG, Koe GS, Middaugh CR. The potential role of proteoglycans in cationic lipid-mediated gene delivery—Studies of the interaction of cationic lipid–DNA complexes with model glycosaminoglycans. J Biol Chem 2001; 276:32806–32813.
156. Zabner J, Fasbender AJ, Moninger T, Poellinger KA, Welsh MJ. Cellular and molecular barriers to gene transfer by a cationic lipid. J Biol Chem 1995; 270:18997–19007.
157. Lin AJ, Slack NL, Ahmad A, Koltover I, George CX, Samuel CE, Safinya CR. Structure and structure-function studies of lipid/plasmid DNA complexes. J. Drug. Targeting 2000; 8: 13–27.
158. Hirsch-Lerner D, Barenholz Y. Probing DNA-cationic lipid interactions with the fluorophore trimethylammonium diphenyl-hexatrien (TMADPH). Biochim Biophys Acta 1998; 1370:17–30.
159. Tang F, Hughes JA. Use of dithiodilycolic acid as a tether for cationic lipids decreases the cytotoxicity and increases transgene expression of plasmid DNA in vitro. Bioconjug. Chem 1999; 10:791–796.
160. Byk G, Wetzer B, Frederic M. Reduction sensitive lipopolyamines as a novel nonviral gene delivery system for modulated release of DNA with improved transgene expression. J Med Chem 2000; 43:4377–4387.
161. Balasubramaniam RP, Bennett MJ, Aberle AM, Malone JG, Nantz MH, Malone RW. Structural and functional analysis of cationic transfection lipids: The hydrophobic domain. Gene Ther 1996; 3:163–172.
162. Weltzer B, Byk G, Frederic M. Reducible cationic lipids for gene transfer. Biochem J 2001; 356:747–756.
163. Zanta MA, Belguise-Valladier P, Behr JP. Gene delivery: A single nuclear locallisation signal is sufficient to carry DNA to the cell nucleus. Proc Natl Acad Sci USA 1999; 96:91–96.
164. Cartier R, Reszka R. Utilization of synthetic peptides containing nuclear localization signal for nonviral gene transfer systems. Gene Ther 2002; 9:157–167.
165. Wheeler JJ, Palmer L, Ossanlou M. Stabilized plasmid-lipid particles: Construction and characterization. Gene Ther 1999; 6:271–281.